Contrib Mineral Petrol (2005) 149: 316–337
DOI 10.1007/s00410-005-0651-1

ORIGINAL PAPER

O. G. Safonov · L. L. Perchuk · Yu. A. Litvin · L. Bindi

# Phase relations in the $CaMgSi_2O_6$–$KAlSi_3O_8$ join at 6 and 3.5 GPa as a model for formation of some potassium-bearing deep-seated mineral assemblages

Received: 18 August 2004 / Accepted: 20 December 2004 / Published online: 3 March 2005


**Abstract** The join $CaMgSi_2O_6$–$KAlSi_3O_8$ has been studied at 6 GPa (890–1,500°C) and 3.5 GPa (1,000–1,100°C). K-rich melts in the join produce assemblages Cpx + Grt, Cpx + Opx, Cpx + San, and Cpx + Grt + San at 1,100–1,300°C. At $N_{San}^{system} < \sim 70$ mol%, sanidine is unstable on the solidus and appears at the liquidus, if $N_{San}^{system} > 90$ mol%. This explains a scarcity of San in mantle Cpx-rich assemblages and its association with high-K aluminosilicate melt inclusions in diamonds. In absence of San, KCpx is the only host for potassium. The K-jadeite content in KCpx systematically increases with decreasing temperature and reaches 10–12 mol% near the solidus. However, KCpx coexists with San at $N_{San}^{system} > 70$ mol% and < 1,300°C, being formed via reaction San + L = KCpx. The KJd content in KCpx is controlled by the equilibrium San = KJd + $SiO_2^L$ that displaces to the right with increasing pressure and decreasing both the temperature and $a_{SiO_2}^L$. This equilibrium is considered to be responsible for the formation of San lamellae in natural UHP Cpx. In our experiments at 3.5 GPa, garnet is absent whereas the KJd and Ca-Eskola contents in Cpx are low, and the join $CaMgSi_2O_6$–$KAlSi_3O_8$ is close to binary (with the eutectic Cpx + San + L). Different topologies of the join at 6 and 3.5 GPa define a sequence of mineral crystallization from K-rich aluminosilicate melts during cooling and decompression: from KCpx + Grt without San at $P > 4$ GPa to Cpx + San at $P < 4$ GPa. Similar sequence of assemblages is observed in some eclogitic xenoliths from kimberlites and Grt–Cpx rocks of the Kokchetav Complex (Northern Kazakhstan).

Editorial Responsibility: T.L. Grove

O. G. Safonov (✉) · Yu. A. Litvin
Institute of Experimental Mineralogy,
Russian Academy of Sciences,
Chernogolovka, Moscow District, 142432, Russia
E-mail: oleg@iem.ac.ru
Tel.: 007-096-52-46205
Fax: 007-096-52-49687

L. L. Perchuk
Department of Geology, Moscow State University,
Vorobievy Gory, Moscow, 119899, Russia

L. Bindi
Dipartimento di Scienze della Terra, University of Firenze,
Via La Pira 4, I-50121, Firenze, Italy

## Abbreviations

### Phases and end-members

| | |
|---|---|
| Ab | albite ($NaAlSi_3O_8$) |
| Ca-Esk | Ca-Eskola pyroxene ($Ca_{0.5}AlSi_2O_6$) |
| Ca-Ts | Ca-Tschermack pyroxene ($CaAl_2SiO_6$) |
| CEn | clinoenstatite ($Mg_2Si_2O_6$) |
| Cos | coesite ($SiO_2$) |
| Cpx | clinopyroxene and $Cpx_{ss}$ solid solution |
| Di | diopside ($CaMgSi_2O_6$) |
| En | orthoenstatite ($Mg_2Si_2O_6$) |
| Fo | forsterite ($Mg_2SiO_4$) |
| Grt | garnet and $Grt_{ss}$ solid solution |
| Grs | grossular ($Ca_3Al_2Si_3O_{12}$) |
| Jd | jadeite ($NaAlSi_2O_6$) |
| KCpx | potassium-bearing clinopyroxene |
| KJd | potassium jadeite ($KAlSi_2O_6$) |
| Ks | kalsilite ($KAlSiO_4$) |
| Ky | kyanite ($Al_2SiO_5$) |
| L | melt |
| Lc | leucite ($KAlSi_2O_6$) |
| Mg-Ts | Mg-Tschermack pyroxene ($MgAl_2SiO_6$) |
| Opx | orthopyroxene and $Opx_{ss}$ its solid solution |
| Prp | pyrope ($Mg_3Al_2Si_3O_{12}$) |
| Q | products of melt quenching |
| San | sanidine ($KAlSi_3O_8$) |
| SWd | Si-wadeite ($K_2Si_4O_9$) |
| Wol | orthowollastonite ($Ca_2Si_2O_6$) |

### Thermodynamic symbols

| | |
|---|---|
| P | pressure |
| T | temperature |

| | |
|---|---|
| $N_{KJd}^{Cpx}$ | molar per cent of KJd in Cpx |
| $N_{Ca}^{Grt}$ | molar per cent of Grs in Grt |
| $a_{SiO_2}^{L}$ | silica activity in a melt |
| $N_{San}^{system}$ | molar per cent of $KAlSi_3O_8$ in a system (starting mixture) |

## Introduction

Sanidine (San) is a very rare mineral in the mantle assemblages. Initial findings of sanidine inclusions in diamonds (e.g., Prinz et al. 1975) were attributed to the parageneses of "uncertain origin" regarding their time of the formation with respect to the host diamond. Further study showed that sanidine in diamonds occurred both as separate inclusions and polyphase inclusions with other minerals. Sanidine prefers eclogitic assemblages, e.g., omphacite, garnet, coesite, and rutile (Bulanova and Argunov 1985; Meyer and McCallum 1986; Novgorodov et al. 1990; Sobolev et al. 1998), whereas only a single its peridotitic parageneses is known (cf. Wang 1998). Sanidine is described in some eclogite xenoliths from kimberlites, i.e., in kyanite-bearing, kyanite–coesite varieties, and grosspydites (Smyth and Hatton 1977; Wohletz and Smyth 1984; Spetsius et al. 1984; Schulze and Helmstaedt 1988; Schulze et al. 2000), as well as in bimineralic (clinopyroxene and garnet, Cpx + Grt) and orthopyroxene-bearing eclogites (Mathias et al. 1970; Reid et al. 1976; Schmickler et al. 2004). The sanidine content in these rocks does not exceed 3–4 vol%. Textural relationships suggest that, in the most cases, sanidine is formed after garnet and clinopyroxene. Large grains of sanidine (Smyth and Hatton 1977; Spetsius et al. 1984) and its occurrence as inclusions in garnets (Schulze and Helmstaedt 1988; Schmickler et al. 2004) are very rare. As a rule, sanidine forms intergranular rims and small grains at the boundaries of clinopyroxenes, garnets, and other minerals. A specific appearance of sanidine in some eclogitic xenoliths are fine (less than 20 μm) lamellae in clinopyroxenes (Reid et al. 1976; Smith et al. 1991; Schmickler et al. 2004), which are locally accompanied by lamellae of garnet, orthopyroxene, and phlogopite. Similar sanidine lamellae are also described in clinopyroxenes of the Grt–Cpx–carbonate rocks of the Kokchetav UHP Complex (Sobolev and Shatsky 1990; Perchuk et al. 1996, 2002, 2003; Zhang et al. 1997; Perchuk and Yapaskurt 1998; Shatsky and Sobolev 2003, Chap. 2.3).

Experimental data indicate that the sanidine is stable up to pressures of 6.2–6.5 GPa in the temperature range 1,000–1,200°C (Kinomura et al. 1975; Urakawa et al. 1994; Yagi et al. 1994; Akaogi et al. 2004). At higher pressures, sanidine decomposes to the assemblage Si-wadeite + kyanite + coesite (SWd + Ky + Cos) (Kinomura et al. 1975; Urakawa et al. 1994; Yagi et al. 1994; Akaogi et al. 2004). Although Ky and Cos are characteristic minerals of sanidine-bearing mantle assemblages, SWd has never been found in their parageneses. Another high-pressure precursor of sanidine might be the hollandite-structured $KAlSi_3O_8$, which is stable at pressures above 9–9.5 GPa (Ringwood et al. 1967; Kinomura et al. 1975; Urakawa et al. 1994; Yagi et al. 1994; Akaogi et al. 2004). Stachel et al. (2000b) reported a unique microcline inclusion in diamond associated with the perovskite-structured $MgSiO_3$ that could imply the initial presence of $KAlSi_3O_8$ hollandite at the time of entrapment. Davies and Harlow (2002) argue that cymrite, $KAlSi_3O_8 \cdot nH_2O$ ($n \leq 1$), might a possible precursor of sanidine at high-pressure under elevated water activity. However, cymrite is stable below 1,000°C at 5–6 GPa (e.g., Thompson et al. 1998; Davies and Harlow 2002), and therefore can be formed only at high-pressure and low-temperature metamorphic conditions (Massone et al. 2000), rather than in high-temperature mantle rocks.

Thus, sanidine could be one of the major potassium concentrators in the mantle under the anhydrous conditions, i.e., in absence of phlogopite or amphibole, at pressures below 6.5 GPa. However, it is unstable within anhydrous olivine-bearing assemblages because of reaction San + 2Fo = Ks + 2En (Wendlandt and Eggler 1980). Natural data indicate that sanidine is stable in eclogitic assemblages. But here, there is a much more abundant competitor of sanidine to accept potassium, namely, potassium-bearing clinopyroxene. Our recent experiments (Safonov et al. 2004) show that the clinopyroxene, crystallizing from potassic aluminosilicate and carbonate–silicate melts at pressure 5–6 GPa contains up to 2 wt% of $K_2O$ increasing up to 5 wt% at pressure 7 GPa (Chudinovskikh et al. 2001; Bindi et al. 2002; Safonov et al. 2002, 2003). On the other hand, the presence of sanidine lamellae in deep-seated clinopyroxenes (Reid et al. 1976; Zhang et al. 1997; Perchuk et al. 1996, 2002, 2003; Schmickler et al. 2004; Shatsky and Sobolev 2003, Chap. 2.3) may suggest the decomposition of potassium-bearing clinopyroxene solid solution by decompression and cooling with the formation of sanidine via the following reaction (Luth 1997):

$$3\mathrm{KJd} + 2\mathrm{Ca} - \mathrm{Esk} = 3\mathrm{San} + \mathrm{Ca} - \mathrm{Ts}. \quad (1)$$

because KCpx may contain both the KJd and Ca-Esk end members. Perchuk and coauthors (Perchuk and Yapaskurt 1998; Perchuk et al. 2002, 2003) studied the Cpx–Grt rocks from the Kokchetav UHP complex and observed no Ca-Esk and Ca-Ts both in the lamellae-free KCpx included in garnets and K-free matrix Cpx crowded with the sanidine lamellae. On the basis of this observation, Perchuk and Yapaspurt (1998) proposed an alternative mechanism for the formation of sanidine lamellae, which is based on the reaction of KCpx with a K–Si-rich melt or fluid:

$$\mathrm{KJd\ (in\ KCpx)} + [\mathrm{SiO_2}]^{\mathrm{L/fl}} = \mathrm{San}. \quad (2)$$

Reactions (1) and (2) imply that high-potassium clinopyroxene would be unstable within the *P–T* field of sanidine stability. Some experimental data (cf. Wang and Takahashi 1999) indicate indeed that the $N_{KJd}^{Cpx}$ abruptly decreases as sanidine appears at pressures below 6.5 GPa. However, detailed experimental data on the relevant stability of sanidine and potassium-bearing clinopyroxene are absent. Because KCpx is an indicator of high potassium activity in the mantle (Harlow 1997; Perchuk et al. 2002), it is very important to know whether the assemblage of potassium-poor clinopyroxene plus sanidine replaces KCpx at the sanidine stability conditions.

The stability of sanidine in the mantle environment is directly related to the problem of origin of the mantle potassium-rich melts included in diamonds (e.g., Navon et al. 2003). A possibility of the sanidine formation from UHP potassic liquids (Wohletz and Smyth 1984; Spetsius et al. 1984; Novgorodov et al. 1990) is supported by data on occurrences of sanidine in the assemblage with inclusions of potassic aluminosilicate melts in diamonds (Bulanova and Argunov 1985; Novgorodov et al. 1990). In addition, the stoicheometry of the K-rich aluminosilicate melts that are included in diamonds is very close to $KAlSi_3O_8$ (Prinz et al. 1975; Bulanova and Argunov 1985; Novgorodov et al. 1990; Shiryaev et al. 2003; Navon et al. 2003). Experiments on the "dry" systems Di–Lc, Di–Lc–Jd, Di–San, Di–San–Jd, and Di–San–Ab at pressures above 5 GPa show that the $SiO_2$-rich melts (> 50 wt%) with $Al_2O_3$ > 10 wt% and $K_2O$ > 10 wt% can readily coexist with KCpx, Opx, Grs-rich Grt, Ky and Cos (Harlow 1999; Safonov et al. 2002, 2003, 2004), which are major minerals coexisting with San in the mantle assemblages.

The join Di–San is the simple system to test the idea of the formation of the San-bearing mantle assemblages from the potassium-rich melts under UHP–HP conditions and to study the relations of sanidine and potassium-bearing clinopyroxene. Detailed investigation of the join Di–San at UHP conditions has not been previously reported, although. At 6 GPa and 1,400°C, Harlow (1999) produced an assemblage of Cpx + Opx + San + K–Al–Si melt from mixtures of natural Di and San. The content of $K_2O$ in Cpx did not exceed 0.2 wt%. Higher $K_2O$ in Cpx (> 1 wt%) was observed by Harlow (1999) at P > 8 GPa in the Cpx + Grt + Ky + SWd assemblage in the sanidine-free field. Thus, the maximum KJd solubility in clinopyroxene in equilibrium with sanidine is unknown. It is still unclear whether garnet is stable in the Di–San join at P < 8 GPa. To expand on the results of Harlow's (1999) preliminary runs, we performed a systematic study of the join Di–San at pressures 6 and 3.5 GPa. The major purposes of our study can be formulated as follows:

1. Determination of the KJd solubility in clinopyroxene near the upper pressure boundary (e.g., 6 GPa) of the sanidine stability.
2. Testing sanidine stability in diopside-rich (e.g., eclogite-like) assemblages.
3. Examination of sanidine formation at expense of KCpx with application to sanidine lamellae in natural clinopyroxenes.
4. Tentative evaluation of a pressure boundary for Grt stability with Cpx + San + L.
5. Study of Cpx composition in equilibrium with K-rich aluminosilicate melt and/or sanidine, i.e., the KJd, Ca-Ts, Ca-Esk, and CEn contents in Cpx as a function of *T* and *P*.

## Starting materials, experimental technique, and analytical procedures

Mixtures of stoichiometric gels of $CaMgSi_2O_6$ and $KAlSi_3O_8$ compositions were used as starting materials. The gels were prepared using the nitrate gelling method (Hamilton and Henderson 1968). After preparation, gels were fired to drive off volatiles and kept in desiccator. The starting gels were mixed under ethanol to produce the desired mixtures (Table 1), and about 20 mg of each mixture were placed into $Pt_{60}Rh_{40}$ capsules of 4 mm in diameter. The capsules with charges were subsequently dried during 12–24 h at 110°C and hermetically sealed by arc-welding. Despite the drying procedure, the starting gel mixtures contained small but uncontrolled amount of water, resulted in the formation of hydrous phases during quenching of melt in the low-temperature experiments (below 1,100°C).

The experiments (Table 1) were performed at 6 GPa and 890–1,500°C and 3.5 GPa and 1,000–1,100°C with the high-pressure "anvil-with-hole" apparatus (Litvin 1991; Safonov et al. 2002, 2003, 2004), which is a modification of the Bridgmen-type anvil assembly (cf. Bradley 1969). The apparatus is characterized by a homogeneous distribution of pressure and temperature (~1°C/mm.) in the reaction volume of 0.1–0.15 $cm^3$, which has been estimated by the special runs on basalt liquidus melting (see details in Litvin 1991). The high-pressure cell was prepared from limestone (Algeti mine, Georgia) individually for each run (Litvin 1991; Safonov et al. 2002, 2003). The cell is equipped with a graphite heater of 7.2 mm in length, 7.5 mm in diameter, and 0.75 mm wall thickness. The capsule was placed in the center of the cell on the holders made of pressed MgO and BN mixture (MgO : BN = 3 : 1). Pressurization of the cell was accomplished using the uni-axial compression of upper and lower anvils in a 500-ton hydraulic press. Pressure at room temperature was calibrated using bismuth phase transitions at 2.55 GPa (Bi I–Bi II), 2.7 GPa, and 7.7 GPa (Bi III–Bi V) (Homan 1975). Pressure was corrected for high temperature with the diamond-graphite curve (Kennedy and Kennedy 1976) using growth/dissolution of diamond seeds in carbon-oversaturated multicomponent carbonate melts (Spivak

**Table 1** Run conditions and products of experiments in the join $CaMgSi_2O_6$–$KAlSi_3O_8$ at 6 and 3.5 GPa

| *P*, GPa | Run number | $N_{San}^{system}$ | Temperature, °C | Time, min | Run products |
|---|---|---|---|---|---|
| 6 | 1160 | 10 | 1,350 | 120 | Cpx, Q |
| | 1195 | 10 | 1,150 | 270 | Cpx, Grt, Q |
| | 1169 | 20 | 1,450 | 30 | Q[b] |
| | 1168 | 20 | 1,350 | 120 | Cpx, Q[b] |
| | 1159 | 20 | 1,200 | 180 | Cpx, Opx[c], Q |
| | 1197 | 20 | 1,150 | 270 | Cpx, Grt[a], Q |
| | 1155 | 20 | 1,070 | 240 | Cpx, Grt[a], Q |
| | 929 | 30 | 1,260 | 240 | Cpx, Opx, Q |
| | 1080 | 30 | 1,140 | 300 | Cpx, Grt, Q |
| | 1035 | 30 | 1,040 | 360 | Cpx, Grt, Q |
| | 1148 | 40 | 1,300 | 120 | Cpx, Grt, Q |
| | 928 | 40 | 1,260 | 240 | Cpx, Grt, glass |
| | 1081 | 40 | 1,140 | 300 | Cpx, Grt, Q |
| | 1082 | 40 | 1,040 | 420 | Cpx, Grt, Q |
| | 950 | 50 | 1,400 | 155 | Cpx, glass |
| | 926 | 50 | 1,310 | 240 | Cpx, glass |
| | 1006 | 50 | 1,110 | 360 | Cpx[c], Grt, glass |
| | 949 | 50 | 1,040 | 365 | Cpx, Grt, Q |
| | 1037 | 50 | 980 | 840 | Cpx, Grt, Q |
| | 1036 | 60 | 1,500 | 20 | Glass |
| | 951 | 60 | 1,350 | 195 | Cpx, glass |
| | 941 | 60 | 1,160 | 300 | Cpx, Grt, glass |
| | 996 | 60 | 1,040 | 360 | Cpx, Grt, glass |
| | 927 | 70 | 1,280 | 240 | Cpx, Grt, Q, glass |
| | 1047 | 70 | 1,240 | 255 | Cpx, Grt, glass |
| | 961 | 70 | 1,130 | 315 | Cpx, Grt, glass |
| | 1005 | 70 | 1,110 | 360 | Cpx, Grt, glass |
| | 1083 | 70 | 1,050 | 420 | Cpx, Grt, Q |
| | 1011 | 80 | 1,380 | 150 | Glass |
| | 1120 | 80 | 1,340 | 30 | Glass |
| | 962 | 80 | 1,290 | 195 | Cpx, Grt, glass |
| | 946 | 80 | 1,250 | 240 | Cpx, Grt, glass |
| | 1121 | 80 | 1,150 | 240 | Cpx, Grt, San, glass |
| | 1024 | 80 | 1,090 | 315 | Cpx, Grt, San[c], Q, glass |
| | 1136 | 80 | 1,000 | 480 | Cpx, Grt, San, Q |
| | 1093 | 85 | 1,420 | 60 | Glass |
| | 1109 | 85 | 1,350 | 30 | Glass |
| | 1086 | 85 | 1,300 | 120 | Cpx, San, Q |
| | 1087 | 85 | 1,200 | 300 | Cpx, San, Q |
| | 1090 | 85 | 1,100 | 360 | Cpx, Grt, San, glass |
| | 1084 | 90 | 1,320 | 150 | San, glass |
| | 1046 | 90 | 1,290 | 240 | Cpx, San, Q, glass |
| | 1088 | 90 | 1,200 | 300 | Cpx, San, Q |
| | 1194 | 90 | 1,160 | 255 | Cpx, San, Q |
| | 1089 | 90 | 1,100 | 360 | Cpx, Grt, San, glass |
| | 978 | 90 | 890 | 785 | Cpx, Grt, San, Q |
| | 1149 | 95 | 1,350 | 60 | San, glass |
| | 1022 | 95 | 940 | 840 | Cpx, San, SWd, Q |
| 3.5 | 1078 | 50 | 1,100 | 300 | *Cpx*, *Q*, glass |
| | 1071 | 60 | 1,110 | 240 | *Cpx*, glass |
| | 1073 | 60 | 1,050 | 360 | *Cpx*, *San*, glass |
| | 1067 | 70 | 1,100 | 240 | *Cpx*, *San*, glass, *Q* |
| | 1072 | 70 | 1,000 | 840 | *Cpx*, *San*, *Q* |
| | 1076 | 90 | 1,060 | 360 | *San*, glass |
| | 1077 | 95 | 1,100 | 300 | *San*, glass [*Cpx*] |

[a]Phase is not surely identified
[b]Quenching products are presented by numerous skeleton crystals of *Cpx* (Fig. 1a)
[c]Phase is characterized by x-ray

and Livin 2004). As a result, run pressure was controlled to ±0.2 GPa. Because of small reaction volume, experiments with the "anvil-with-hole" assembly cannot be monitored directly with thermocouples. Therefore, the power setting control of temperature has been used (Litvin 1991). The temperature-current power dependence of the cell was calibrated using a $Pt_{70}Rh_{30}/Pt_{94}Rh_6$ thermocouple without pressure correction. The cells were recalibrated after several runs to check the reproducibility of the temperature–current power dependence. Run temperature was controlled within ±20°C using a MINITHERM-300.31 controller.

The experiments started with pressurization at ambient temperature to the desired values during 15–20 min, depending on the target pressure. Subsequently, the charge was heated to the desired temperature in a time period 10–15 min. Duration of each experiment varied in dependence on temperature (Table 1).

**Table 2** Mean composition of phases produced in the join $CaMgSi_2O_6$-$KAlSi_3O_8$ at 6 and 3.5 GPa

| Experiment (Table 1) | 1160 | | | 1195 | | 1159 | |
|---|---|---|---|---|---|---|---|
| Phase | Cpx | glass [a] | Cpx [b] | Cpx | Grt | Cpx | Opx |
| Number of points | 7 | 6 | 1 | 10 | 4 | 25 | 6 |
| $SiO_2$ | 55.37 | 79.57 | 55.92 | 54.97 | 41.71 | 55.69 | 59.13 |
| $Al_2O_3$ | 0.34 | 8.30 | 1.33 | 1.16 | 22.57 | 1.27 | 1.23 |
| MgO | 20.19 | 0.21 | 20.44 | 18.28 | 11.84 | 20.44 | 37.76 |
| CaO | 23.96 | 0.97 | 22.26 | 25.36 | 23.97 | 22.43 | 1.73 |
| $K_2O$ | 0.04 | 11.00 | 0.00 | 0.11 | 0.01 | 0.28 | 0.06 |
| Total | 99.90 | 100.05 | 99.95 | 99.88 | 100.10 | 100.11 | 99.91 |
| Formula ratio per given O | | | | | | | |
| O | 6 | 24 | 6 | 6 | 12 | 6 | |
| Si | 1.986 | 10.482 | 1.991 | 1.979 | 3.010 | 1.988 | 1.988 |
| Al | 0.014 | 1.290 | 0.056 | 0.049 | 1.917 | 0.053 | 0.048 |
| Mg | 1.081 | 0.031 | 1.084 | 0.983 | 1.264 | 1.086 | 1.887 |
| Ca | 0.920 | 0.136 | 0.849 | 0.981 | 1.860 | 0.855 | 0.062 |
| K | 0.000 | 1.850 | 0.000 | 0.002 | 0.000 | 0.010 | 0.000 |
| Total | 4.001 | 13.789 | 3.980 | 3.994 | 8.051 | 3.992 | 3.985 |
| Compositional parameters of pyroxenes and garnets[c] | | | | | | | |
| $Al^{IV}$ | 0.014 | | 0.009 | 0.021 | | 0.012 | 0.002 |
| $Al^{M2}$ | 0.000 | | 0.047 | 0.029 | | 0.038 | 0.046 |
| $Mg^{M2}$ | 0.077 | | 0.132 | 0.016 | | 0.125 | |
| $\square^{M2}$ | 0.000 | | 0.019 | 0.001 | | 0.007 | |
| $N_{Ca}^{Grt}$ | | | | | 59.5 | | |
| End-members in the clinopyroxene solid solution in addition to diopside (mol%)[d] | | | | | | | |
| KJd | 0.0 | | 0.0 | 0.2 | | 1.0 | |
| Ca-Ts | 1.4 | | 0.9 | 2.1 | | 1.2 | |
| Ca-Esk | 0.0 | | 3.8 | 0.2 | | 1.4 | |
| CEn | 7.7 | | 13.2 | 1.6 | | 12.5 | |

| Experiment (Table 1) | 929 | | | 1035 | | | |
|---|---|---|---|---|---|---|---|
| Phase | Cpx | glass | Opx | Cpx | Cpx [e] | Grt | Q |
| Number of points | 8 | 1 | 6 | 20 | 1 | 10 | 5 |
| $SiO_2$ | 55.89 | 71.33 | 57.38 | 55.48 | 51.00 | 44.87 | 55.81 |
| $Al_2O_3$ | 2.31 | 13.95 | 1.71 | 1.89 | 10.28 | 23.10 | 19.28 |
| MgO | 18.49 | 0.73 | 36.24 | 17.99 | 20.42 | 23.23 | 9.75 |
| CaO | 22.09 | 0.57 | 1.70 | 23.66 | 17.87 | 8.75 | 0.09 |
| $K_2O$ | 1.23 | 13.36 | 0.17 | 0.92 | 0.40 | 0.00 | 12.25 |
| Total | 100.01 | 99.94 | 97.20 | 99.94 | 99.97 | 99.95 | 97.18 |
| Formula ratio per given O | | | | | | | |
| O | 6 | 24 | 6 | 6 | 6 | 12 | 24 |
| Si | 1.998 | 9.638 | 1.982 | 1.992 | 1.800 | 3.084 | 7.963 |
| Al | 0.097 | 2.220 | 0.070 | 0.080 | 0.428 | 1.871 | 3.241 |
| Mg | 0.984 | 0.160 | 1.865 | 0.962 | 1.074 | 2.379 | 2.072 |
| Ca | 0.846 | 0.082 | 0.063 | 0.910 | 0.675 | 0.644 | 0.014 |
| K | 0.055 | 2.302 | 0.008 | 0.042 | 0.019 | 0.004 | 2.229 |
| Total | 3.981 | 14.403 | 3.987 | 3.987 | 3.996 | 7.982 | 15.519 |
| Compositional parameters of pyroxenes and garnets[c] | | | | | | | |
| $Al^{IV}$ | 0.002 | | 0.018 | 0.008 | 0.200 | | |
| $Al^{M2}$ | 0.095 | | 0.052 | 0.072 | 0.228 | | |
| $Mg^{M2}$ | 0.080 | | | 0.035 | 0.301 | | |
| $\square^{M2}$ | 0.019 | | | 0.013 | 0.004 | | |
| $N_{Ca}^{Grt}$ | | | | | | 21.3 | |
| End-members in the clinopyroxene solid solution in addition to diopside (mol%) | | | | | | | |
| KJd | 5.5 | | | 4.2 | 1.9 | | |
| Ca-Ts | 0.2 | | | 0.8 | 20.0 | | |
| Ca-Esk | 3.8 | | | 2.6 | 0.8 | | |
| CEn | 8.0 | | | 3.5 | 30.1 | | |

| Experiment (Table 1) | 950 | | 1006 | | | 1037 | | |
|---|---|---|---|---|---|---|---|---|
| Phase | Cpx | glass | Cpx | glass | Grt | Cpx | Grt | Q |
| Number of points | 20 | 2 | 14 | 4 | 5 | 4 | 2 | 1 |
| $SiO_2$ | 55.31 | 67.36 | 55.20 | 66.45 | 44.05 | 55.04 | 39.58 | 64.62 |

**Table 2** (Contd.)

| Experiment (Table 1) | 950 | | 1006 | | | 1037 | | |
|---|---|---|---|---|---|---|---|---|
| Phase | Cpx | glass | Cpx | glass | Grt | Cpx | Grt | Q |
| $Al_2O_3$ | 1.61 | 14.73 | 3.49 | 14.62 | 23.86 | 1.97 | 21.97 | 16.04 |
| MgO | 20.17 | 1.89 | 18.37 | 1.69 | 21.00 | 15.97 | 1.26 | 1.26 |
| CaO | 22.64 | 1.35 | 22.27 | 1.49 | 11.02 | 24.95 | 36.35 | 2.69 |
| $K_2O$ | 0.21 | 14.67 | 0.58 | 15.74 | 0.08 | 1.70 | 0.06 | 12.39 |
| Total | 99.94 | 100.00 | 99.91 | 99.99 | 100.01 | 99.63 | 99.22 | 97.00 |
| Formula ratio per given O | | | | | | | | |
| O | 6 | 24 | 6 | 24 | 12 | 6 | 12 | 24 |
| Si | 1.976 | 9.271 | 1.969 | 9.223 | 3.048 | 1.995 | 2.980 | 9.110 |
| Al | 0.068 | 2.389 | 0.147 | 2.392 | 1.945 | 0.084 | 1.949 | 2.664 |
| Mg | 1.073 | 0.387 | 0.976 | 0.350 | 2.165 | 0.862 | 0.142 | 0.264 |
| Ca | 0.866 | 0.200 | 0.851 | 0.222 | 0.816 | 0.968 | 2.932 | 0.407 |
| K | 0.010 | 2.574 | 0.027 | 2.786 | 0.007 | 0.078 | 0.001 | 2.227 |
| Total | 3.993 | 14.821 | 3.968 | 14.972 | 7.982 | 3.987 | 8.004 | 14.672 |
| Compositional parameters of pyroxenes and garnets | | | | | | | | |
| $Al^{IV}$ | 0.024 | | 0.031 | | | 0.005 | | |
| $Al^{M2}$ | 0.044 | | 0.115 | | | 0.079 | | |
| $Mg^{M2}$ | 0.117 | | 0.091 | | | 0.000 | | |
| $\square^{M2}$ | 0.007 | | 0.032 | | | 0.000 | | |
| $N_{Ca}^{Grt}$ | | | | | 27.4 | | | |
| End-members in the clinopyroxene solid solution in addition to diopside (mol%) | | | | | | | | |
| KJd | 1.0 | | 2.7 | | | 7.8 | | |
| Ca-Ts | 2.4 | | 3.1 | | | 0.5 | | |
| Ca-Esk | 1.4 | | 6.4 | | | 0.0 | | |
| CEn | 11.7 | | 9.1 | | | 0.0 | | |

| Experiment (Table 1) | 951 | | 996 | | | 927 | | | |
|---|---|---|---|---|---|---|---|---|---|
| Phase | Cpx | glass | Cpx | Grt | glass | Cpx | glass | Grt | Q |
| Number of points | 3 | 1 | 7 | 2 | 3 | 15 | 6 | 7 | 1 |
| $SiO_2$ | 56.06 | 63.47 | 55.47 | 45.17 | 68.04 | 54.84 | 67.85 | 43.42 | 66.30 |
| $Al_2O_3$ | 1.75 | 15.17 | 1.99 | 24.17 | 14.36 | 3.48 | 14.95 | 23.60 | 15.05 |
| MgO | 21.59 | 2.72 | 17.56 | 25.56 | 0.81 | 17.14 | 1.41 | 20.00 | 1.49 |
| CaO | 20.19 | 2.17 | 23.24 | 4.82 | 0.41 | 23.76 | 1.15 | 12.73 | 1.04 |
| $K_2O$ | 0.14 | 16.34 | 1.22 | 0.14 | 16.15 | 0.76 | 15.60 | 0.05 | 15.92 |
| Total | 99.73 | 99.87 | 99.48 | 99.86 | 99.77 | 99.98 | 100.96 | 99.80 | 99.80 |
| Formula ratio per given O | | | | | | | | | |
| O | 6 | 24 | 6 | 12 | 24 | 6 | 24 | 12 | 24 |
| Si | 1.984 | 8.925 | 1.995 | 3.070 | 9.397 | 1.967 | 9.255 | 3.027 | 9.201 |
| Al | 0.073 | 2.513 | 0.084 | 1.936 | 2.339 | 0.148 | 2.437 | 1.939 | 2.461 |
| Mg | 1.137 | 0.570 | 0.935 | 2.588 | 0.166 | 0.915 | 0.290 | 2.076 | 0.329 |
| Ca | 0.765 | 0.326 | 0.894 | 0.351 | 0.060 | 0.912 | 0.170 | 0.950 | 0.169 |
| K | 0.006 | 2.929 | 0.056 | 0.012 | 2.844 | 0.035 | 2.752 | 0.022 | 2.818 |
| Total | 3.965 | 15.263 | 3.964 | 7.957 | 14.806 | 3.977 | 14.903 | 8.015 | 14.977 |
| Compositional parameters of pyroxenes and garnets | | | | | | | | | |
| $Al^{IV}$ | 0.016 | | 0.005 | | | 0.033 | | | |
| $Al^{M2}$ | 0.057 | | 0.079 | | | 0.114 | | | |
| $Mg^{M2}$ | 0.201 | | 0.019 | | | 0.030 | | | |
| $\square^{M2}$ | 0.021 | | 0.018 | | | 0.023 | | | |
| $N_{Ca}^{Grt}$ | | | | 12.0 | | | | 31.4 | |
| End-members in the clinopyroxene solid solution in addition to diopside (mol%) | | | | | | | | | |
| KJd | 0.6 | | 5.6 | | | 3.5 | | | |
| Ca-Ts | 1.6 | | 0.5 | | | 3.3 | | | |
| Ca-Esk | 4.2 | | 3.6 | | | 4.6 | | | |
| CEn | 20.1 | | 1.9 | | | 3.0 | | | |

| Experiment (Table 1) | 1005 | | | 946 | | | 1109 | 1084 |
|---|---|---|---|---|---|---|---|---|
| Phase | Cpx | glass | Grt | Cpx | glass | Grt | glass | glass |
| Number of points | 6 | 2 | 2 | 9 | 3 | 5 | 5 | 4 |
| $SiO_2$ | 55.30 | 67.44 | 44.10 | 55.69 | 65.03 | 43.85 | 67.06 | 65.75 |
| $Al_2O_3$ | 1.77 | 13.49 | 24.31 | 2.81 | 14.44 | 23.55 | 15.74 | 17.18 |
| MgO | 18.82 | 2.14 | 23.56 | 16.18 | 1.20 | 20.14 | 2.94 | 1.00 |

**Table 2** (Contd.)

| Experiment (Table 1) | 1005 | | | 946 | | | 1109 | 1084 |
|---|---|---|---|---|---|---|---|---|
| Phase | Cpx | glass | Grt | Cpx | glass | Grt | glass | glass |
| CaO | 23.54 | 2.07 | 8.00 | 23.50 | 1.33 | 12.15 | 3.43 | 1.32 |
| $K_2O$ | 0.35 | 14.63 | 0.02 | 1.55 | 17.92 | 0.25 | 15.23 | 14.74 |
| Total | 99.78 | 99.77 | 100.00 | 99.73 | 99.91 | 99.94 | 104.40 | 99.99 |
| Formula ratio per given O | | | | | | | | |
| O | 6 | 24 | 12 | 6 | 24 | 12 | 24 | 24 |
| Si | 1.984 | 9.319 | 3.026 | 2.000 | 9.164 | 3.049 | 8.956 | 9.060 |
| Al | 0.075 | 2.197 | 1.966 | 0.119 | 2.397 | 1.930 | 2.477 | 2.790 |
| Mg | 1.006 | 0.441 | 2.409 | 0.867 | 0.252 | 2.086 | 0.585 | 0.205 |
| Ca | 0.905 | 0.306 | 0.588 | 0.906 | 0.200 | 0.905 | 0.491 | 0.195 |
| K | 0.016 | 2.577 | 0.002 | 0.071 | 3.222 | 0.022 | 2.593 | 2.590 |
| Total | 3.986 | 14.840 | 7.992 | 3.963 | 15.236 | 7.992 | 15.102 | 14.840 |
| Compositional parameters of pyroxenes and garnets | | | | | | | | |
| $Al^{IV}$ | 0.016 | | | 0.000 | | | | |
| $Al^{M2}$ | 0.059 | | | 0.119 | | | | |
| $Mg^{M2}$ | 0.065 | | | 0.000 | | | | |
| $\square^{M2}$ | 0.014 | | | 0.023 | | | | |
| $N_{Ca}^{Grt}$ | | | 19.6 | | | 30.3 | | |
| End-members in the clinopyroxene solid solution in addition to diopside (mol%) | | | | | | | | |
| KJd | 1.6 | | | 7.1 | | | | |
| Ca-Ts | 1.6 | | | 0.0 | | | | |
| Ca-Esk | 2.8 | | | 4.6 | | | | |
| CEn | 6.5 | | | 0.0 | | | | |

| Experiment (Table 1) | 1024 | | | | | 1086 | | |
|---|---|---|---|---|---|---|---|---|
| Phase | Cpx | glass | Grt | San | Q | Cpx | San | Q |
| Number of points | 17 | 8 | 8 | 9 | 3 | 12 | 5 | 3 |
| $SiO_2$ | 55.65 | 68.14 | 44.12 | 64.39 | 66.78 | 55.34 | 65.30 | 63.09 |
| $Al_2O_3$ | 2.08 | 14.71 | 23.74 | 17.87 | 15.14 | 0.00 | 18.28 | 15.50 |
| MgO | 18.04 | 0.74 | 21.56 | 0.02 | 0.59 | 18.61 | 0.00 | 0.67 |
| CaO | 22.92 | 0.41 | 10.31 | 0.02 | 0.24 | 26.13 | 0.07 | 1.01 |
| $K_2O$ | 1.03 | 15.97 | 0.18 | 17.67 | 17.26 | 0.20 | 16.84 | 15.71 |
| Total | 99.73 | 99.98 | 99.92 | 99.96 | 100.01 | 100.30 | 100.49 | 95.98 |
| Formula ratio per given O | | | | | | | | |
| O | 6 | 24 | 12 | 8 | 24 | 6 | 8 | 24 |
| Si | 1.999 | 9.397 | 3.051 | 3.000 | 9.293 | 1.994 | 3.007 | 9.139 |
| Al | 0.088 | 2.391 | 1.934 | 0.981 | 2.482 | 0.000 | 0.992 | 2.647 |
| Mg | 0.965 | 0.152 | 2.221 | 0.001 | 0.122 | 0.999 | 0.000 | 0.144 |
| Ca | 0.881 | 0.061 | 0.764 | 0.001 | 0.036 | 1.008 | 0.003 | 0.156 |
| K | 0.047 | 2.809 | 0.016 | 1.050 | 3.063 | 0.009 | 0.989 | 2.903 |
| Total | 3.981 | 14.814 | 7.996 | 5.037 | 14.997 | 4.011 | 4.991 | 14.989 |
| Compositional parameters of pyroxenes and garnets | | | | | | | | |
| $Al^{IV}$ | 0.001 | | | | | 0.006 | | |
| $Al^{M2}$ | 0.087 | | | | | 0.000 | | |
| $Mg^{M2}$ | 0.052 | | | | | 0.000 | | |
| $\square^{M2}$ | 0.019 | | | | | 0.000 | | |
| $N_{Ca}^{Grt}$ | | | 25.6 | | | | | |
| End-members in the clinopyroxene solid solution in addition to diopside (mol%) | | | | | | | | |
| KJd | 4.7 | | | | | 0.0 | | |
| Ca-Ts | 0.1 | | | | | 0.0 | | |
| Ca-Esk | 3.8 | | | | | 0.0 | | |
| CEn | 5.2 | | | | | 0.0 | | |

| Experiment (Table 1) | 1087 [f] | | | | 1088 | | |
|---|---|---|---|---|---|---|---|
| Phase | Di | KCpx | San | Q | Cpx | San | Q |
| Number of points | 19 | 9 | 7 | 2 | 9 | 4 | 4 |
| $SiO_2$ | 55.45 | 54.56 | 65.44 | 66.12 | 55.45 | 65.82 | 64.86 |
| $Al_2O_3$ | 0.03 | 4.04 | 18.29 | 15.39 | 0.00 | 18.27 | 14.54 |
| MgO | 18.98 | 16.92 | 0.01 | 0.89 | 18.55 | 0.03 | 0.54 |
| CaO | 25.41 | 23.59 | 0.03 | 1.08 | 26.62 | 0.03 | 1.11 |
| $K_2O$ | 0.10 | 0.91 | 16.33 | 16.55 | 0.17 | 17.30 | 16.18 |
| Total | 99.98 | 100.02 | 100.10 | 100.01 | 100.79 | 101.44 | 97.23 |

**Table 2** (Contd.)

| Experiment (Table 1) | 1087 [f] | | | | 1088 | | |
|---|---|---|---|---|---|---|---|
| Phase | Di | KCpx | San | Q | Cpx | San | Q |
| Formula ratio per given O | | | | | | | |
| O | 6 | 6 | 8 | 24 | 6 | 8 | 24 |
| Si | 1.998 | 1.957 | 3.014 | 9.201 | 1.991 | 3.008 | 9.281 |
| Al | 0.001 | 0.171 | 0.993 | 2.523 | 0.000 | 0.984 | 2.451 |
| Mg | 1.019 | 0.903 | 0.000 | 0.183 | 0.992 | 0.002 | 0.116 |
| Ca | 0.981 | 0.906 | 0.002 | 0.161 | 1.023 | 0.001 | 0.169 |
| K | 0.006 | 0.042 | 0.959 | 2.937 | 0.008 | 1.008 | 2.953 |
| Total | 4.004 | 3.979 | 4.969 | 15.005 | 4.014 | 5.004 | 14.970 |
| Compositional parameters of pyroxenes and garnets | | | | | | | |
| $Al^{IV}$ | 0.002 | 0.043 | | | 0.009 | | |
| $Al^{M2}$ | 0.000 | 0.128 | | | 0.000 | | |
| $Mg^{M2}$ | 0.019 | 0.031 | | | 0.000 | | |
| $\square^{M2}$ | 0.000 | 0.021 | | | 0.000 | | |
| $N_{Ca}^{Grt}$ | | | | | | | |
| End-members in the clinopyroxene solid solution in addition to diopside (mol%) | | | | | | | |
| KJd | 0.0 | 4.2 | | | 0.0 | | |
| Ca-Ts | 0.0 | 4.3 | | | 0.0 | | |
| Ca-Esk | 0.0 | 4.2 | | | 0.0 | | |
| CEn | 1.9 | 3.1 | | | 0.0 | | |

| Run sample (Table 1) | 1090 [f] | | | | | | | | 1046 | | |
|---|---|---|---|---|---|---|---|---|---|---|---|
| Phase | KCpx | Al-Cpx | Di | glass | Grt | Ca-Grt | San | Q [g] | Cpx | San | glass |
| Number of points | 2 | 14 | 18 | 7 | 11 | 4 | 5 | 1 | 5 | 3 | 5 |
| $SiO_2$ | 55.26 | 52.56 | 55.33 | 56.07 | 42.65 | 42.15 | 65.14 | 70.01 | 55.59 | 64.64 | 65.80 |
| $Al_2O_3$ | 2.02 | 4.97 | 0.01 | 17.05 | 23.34 | 22.67 | 18.36 | 11.25 | 3.00 | 17.88 | 14.94 |
| MgO | 17.46 | 16.62 | 18.80 | 1.48 | 17.67 | 12.39 | 0.00 | 0.26 | 17.99 | 0.11 | 0.64 |
| CaO | 24.30 | 25.62 | 25.76 | 2.62 | 16.29 | 22.60 | 0.13 | 1.31 | 21.69 | 0.04 | 0.58 |
| $K_2O$ | 0.93 | 0.22 | 0.08 | 22.76 | 0.05 | 0.06 | 16.34 | 17.15 | 1.25 | 16.98 | 18.16 |
| Total | 99.97 | 99.99 | 99.98 | 99.98 | 99.98 | 99.86 | 99.97 | 99.98 | 99.52 | 99.65 | 100.12 |
| Formula ratio per given O | | | | | | | | | | | |
| O | 6 | 6 | 6 | 24 | 12 | 12 | 8 | 24 | 6 | 8 | 24 |
| Si | 1.974 | 1.887 | 2.000 | 8.504 | 3.005 | 3.051 | 3.032 | 9.733 | 1.991 | 3.008 | 9.232 |
| Al | 0.108 | 0.257 | 0.000 | 3.037 | 1.937 | 1.873 | 0.958 | 1.843 | 0.127 | 0.980 | 2.462 |
| Mg | 0.913 | 0.862 | 1.008 | 0.187 | 1.854 | 1.380 | 0.000 | 0.054 | 0.960 | 0.008 | 0.134 |
| Ca | 0.954 | 0.972 | 0.993 | 0.155 | 1.229 | 1.702 | 0.019 | 0.195 | 0.832 | 0.002 | 0.087 |
| K | 0.048 | 0.015 | 0.000 | 4.189 | 0.005 | 0.015 | 0.960 | 3.041 | 0.057 | 1.008 | 3.254 |
| Total | 3.996 | 3.992 | 4.000 | 16.072 | 8.029 | 8.020 | 4.969 | 14.866 | 3.967 | 5.006 | 15.169 |
| Compositional parameters of pyroxenes and garnets | | | | | | | | | | | |
| $Al^{IV}$ | 0.026 | 0.113 | 0.000 | | | | | | 0.009 | | |
| $Al^{M2}$ | 0.082 | 0.144 | 0.000 | | | | | | 0.118 | | |
| $Mg^{M2}$ | 0.000 | 0.013 | 1.000 | | | | | | 0.079 | | |
| $\square^{M2}$ | 0.000 | 0.008 | 0.000 | | | | | | 0.033 | | |
| $N_{Ca}^{Grt}$ | | | | | 39.9 | 55.2 | | | | | |
| End-members in the clinopyroxene solid solution in addition to diopside (mol%) | | | | | | | | | | | |
| KJd | 4.8 | 1.5 | 0.0 | | | | | | 5.7 | | |
| Ca-Ts | 2.6 | 11.3 | 0.0 | | | | | | 0.9 | | |
| Ca-Esk | 0.0 | 1.6 | 0.0 | | | | | | 6.6 | | |
| CEn | 0.0 | 1.3 | 0.0 | | | | | | 7.9 | | |

| Experiment (Table 1) | 1022 | | | 978 | | |
|---|---|---|---|---|---|---|
| Phase | Cpx [h] | San | SWd | Cpx [h] | Grt | Q |
| Number of points | 1 | 3 | 3 | 1 | 3 | 3 |
| $SiO_2$ | 56.63 | 66.97 | 72.63 | 55.91 | 39.88 | 64.69 |
| $Al_2O_3$ | 4.45 | 18.55 | 5.79 | 3.54 | 21.82 | 14.92 |
| MgO | 14.47 | 0.02 | 0.85 | 15.32 | 4.52 | 0.10 |
| CaO | 20.36 | 0.04 | 0.52 | 22.50 | 33.54 | 0.48 |
| $K_2O$ | 2.62 | 14.97 | 23.71 | 2.72 | 0.08 | 16.49 |
| Total | 98.53 | 100.56 | 103.50 | 99.99 | 101.84 | 96.68 |

**Table 2** (Contd.)

| Experiment (Table 1) | 1022 | | | 978 | | |
|---|---|---|---|---|---|---|
| Phase | Cpx [h] | San | SWd | Cpx [h] | Grt | Q |
| O | 6 | 8 | 9 | 6 | 12 | 24 |
| Si | 2.028 | 3.038 | 3.791 | 2.012 | 2.972 | 9.301 |
| Al | 0.188 | 0.991 | 0.356 | 0.150 | 1.916 | 2.528 |
| Mg | 0.772 | 0.002 | 0.066 | 0.821 | 0.502 | 0.021 |
| Ca | 0.781 | 0.002 | 0.029 | 0.867 | 2.677 | 0.074 |
| K | 0.119 | 0.866 | 1.578 | 0.125 | 0.008 | 3.024 |
| Total | 3.887 | 4.899 | 5.820 | 3.975 | 8.075 | 14.948 |
| Compositional parameters of pyroxenes and garnets | | | | | | |
| $Al^{IV}$ | 0.000 | | | 0.000 | | |
| $Al^{M2}$ | 0.188 | | | 0.150 | | |
| $Mg^{M2}$ | 0.000 | | | 0.000 | | |
| $\square^{M2}$ | 0.100 | | | 0.008 | | |
| $N_{Ca}^{Grt}$ | | | | | 84.2 | |
| End-members in the clinopyroxene solid solution in addition to diopside (mol%) | | | | | | |
| KJd | 11.9 | | | 12.5 | | |
| Ca-Ts | 0.0 | | | 0.0 | | |
| Ca-Esk | 20.0 | | | 1.6 | | |
| CEn | 0.0 | | | 0.0 | | |

| Experiment (Table 1) | 1067 | | | 1072 | | |
|---|---|---|---|---|---|---|
| Phase | glass | Cpx | San | Q | Cpx [h] | San |
| Number of points | 5 | 9 | 3 | 2 | 3 | 7 |
| $SiO_2$ | 65.74 | 55.35 | 65.07 | 72.47 | 57.28 | 65.18 |
| $Al_2O_3$ | 16.00 | 1.10 | 18.15 | 10.70 | 1.26 | 17.91 |
| MgO | 1.27 | 20.18 | 0.00 | 0.50 | 18.29 | 0.31 |
| CaO | 1.04 | 23.21 | 0.00 | 0.10 | 22.58 | 0.45 |
| $K_2O$ | 15.80 | 0.17 | 16.76 | 12.43 | 0.61 | 16.12 |
| Total | 99.85 | 100.01 | 99.98 | 96.2 | 100.01 | 99.97 |
| Formula ratio per given O | | | | | | |
| O | 24 | 6 | 8 | 24 | 6 | 8 |
| Si | 9.128 | 1.981 | 3.010 | 10.075 | 2.038 | 3.009 |
| Al | 2.618 | 0.046 | 0.989 | 1.753 | 0.053 | 0.974 |
| Mg | 0.263 | 1.076 | 0.000 | 0.104 | 0.970 | 0.021 |
| Ca | 0.155 | 0.889 | 0.000 | 0.015 | 0.861 | 0.024 |
| K | 2.798 | 0.007 | 0.990 | 2.204 | 0.028 | 0.949 |
| Total | 14.962 | 3.999 | 4.989 | 14.151 | 3.949 | 4.978 |
| Compositional parameters of pyroxenes | | | | | | |
| $Al^{IV}$ | | 0.019 | | | 0.000 | |
| $Al^{M2}$ | | 0.027 | | | 0.053 | |
| $Mg^{M2}$ | | 0.103 | | | 0.039 | |
| $\square^{M2}$ | | 0.000 | | | 0.073 | |
| End-members in the clinopyroxene solid solution in addition to diopside (mol%) | | | | | | |
| KJd | | 0.7 | | | 2.8 | |
| Ca-Ts | | 1.9 | | | 0.0 | |
| Ca-Esk | | 0.0 | | | 14.6 | |
| CEn | | 10.3 | | | 3.9 | |

[a]Experiment 1160—residual glass in quench
[b]Experiment 1160—dendritic clinopyroxene in quench
[c]Components in the sites of clinopyroxenes were calculated using the following scheme: $Al^{IV} = 2 - (Si)$, if $(Si) \leq 2$ a.p.f.u., and $Al^{IV} = 0$, if $(Si) > 2$ a.p.f.u. (i.e., assuming that Si occupies exclusively the tetrahedral site, while the Si content above 2.0 a.p.f.u. results from poor-quality analyses of tiny crystals); $Al^{VI} = (Al) - Al^{IV}$; $Mg^{M1} = 1 - Al^{M1}$; $Mg^{M2} = (Mg) - Mg^{M1}$; $\square^{M2} = 1 - (Ca) - (K) - Mg^{M2}$, where elements in parentheses denote atoms in formula unit based on 6 oxygen atoms. Molar per cent of grossular component in garnet is calculated with following formula: $N_{Ca}^{Grt} = Ca/(Ca + Mg)$, where elements denote atoms in formula unit based on 12 oxygen atoms
[d]End-members (mol%) of clinopyroxene solid solution were calculated using the following procedure: KJd = (K)*100, if (K) > (Al) - $Al^{IV}$, unless KJd is assumed to be zero; Ca-Ts = $Al^{IV}$*100; CEn = $Mg^{M2}$*100; Ca-Esk = (2*$\square^{M2}$)*100
[e]Inclusion in garnet
[f]Compositional types of clinopyroxenes and garnets in the experiments 1087 and 1090
[g]Quench in the sanidine-clinopyroxene cumulates (see lower inset in Fig. 1e)
[h]The Si content above 2.0 a.p.f.u. and high Ca-Esk contents result from poor-quality analyses of acicular crystals
Abbreviations: KCpx, potassium-bearing clinopyroxene; Al-Cpx, Ca-Ts-rich clinopyroxene at contacts with garnet; Di, KJd-free clinopyroxene; Grt, centers of garnet grains; Ca-Grt, garnet at the contact with clinopyroxene

Experiments were quenched by shutting power off and subsequently depressurized.

Each run sample was divided into several pieces. This procedure helps to examine thoroughly textural features of run products, which are texturally heterogeneous in some cases (see below). The pieces were embedded in epoxy and polished. After preliminary examination in reflected light, the microscopic features of run products and phase compositions (Table 2) were studied by means of BSE with a CamScan MV2300 (VEGA TS 5130MM) electron microscope equipped with the EDS electron microprobe Link INCA Energy at the RSMA laboratory of the Institute of Experimental Mineralogy. Some samples were examined twice or thrice after repeated polishing. Microprobe analyses were performed at 20 kV accelerating potential, 10 nA of beam current and beam diameter of 3 μm. Microprobe analyses of glass (or the products of quenching) were made using a defocused beam or scanning of area 10×10 μm. The following standards were used: synthetic $SiO_2$ for Si, synthetic MgO for Mg, synthetic $Al_2O_3$ for Al, natural wollastonite for Ca, and natural microcline for K. The ZAF matrix correction was used. No normalization procedure is applied. Mineral formulae (Table 2) were calculated on the basis of a specified number of oxygen atoms.

Hand-picked crystal fragments of Opx from the run product 1159, and Cpx from the run products 1006 and 927, were used for the X-ray single-crystal diffraction studies. Intensity data were collected on an automated diffractometer (Enraf Nonius—CAD4) using Mo Kα radiation monochromatized by a flat graphite crystal. Both the intensity corrections and the strategies of the crystal structure refinements were similar to those carried out in our previous studies (Bindi et al. 2002, 2003). Unit-cell parameters of Opx (space group *Pbca*), determined by centering 25 high-$\theta$ (20–27°) reflections, are: $a = 18.234(2)$ Å, $b = 8.816(1)$ Å, $c = 5.192(1)$ Å. Unit-cell parameters for the two clinopyroxene crystals (space group $C2/c$), determined by centering the same set of 25 high-$\theta$ (20–28°) reflections, are: $a = 9.714(1)$ Å, $b = 8.916(1)$ Å, $c = 5.252(1)$ Å, $\beta = 105.93(1)°$, $V = 437.4(2)$ Å$^3$ and $a = 9.725(1)$ Å, $b = 8.915(1)$ Å, $c = 5.258(1)$ Å, $\beta = 106.02(1)°$, $V = 438.2(2)$ Å$^3$ for the crystals from 1006 and 927 run product, respectively. Several grains of $KAlSi_3O_8$ were hand-picked from the run product 1024, finely ground in an agate mortar, and prepared as a thin layer on a silicon single-crystal. Step-scan powder diffraction data, with 0.02° as step and 9 s as counting time, were recorded with an automated diffractometer (Philips) in the 2$\theta$ range 2–70° using Cu Kα radiation and silicon powder (NBS 640a) as external standard. Detailed examination of the observed pattern shows the absence of diffraction peaks belonging to any crystalline phase other than high sanidine.

The Raman analyses of glasses in order to verify the presence of water were performed using the RM-1000 micro-Raman spectrometer. The samples were exited at room temperature with the 514-nm line of Ar-laser. The magnification of the objective was 50×.

## Experimental results

### Textural relationships in the run products

The run conditions and results of each experiment are presented in Table 1. Textures in the experiments produced at 1,300–1,450°C at the $CaMgSi_2O_6$ content in the system >70 mol% are ambiguous because of spectacular dendritic clinopyroxene crystals (Fig. 1a), which are interpreted as quenched crystals. Orthopyroxene in the experiments 929 and 1159 (Table 1) forms large (up to 50 μm) crystals, which locally contain minute clinopyroxene inclusions (Fig. 1b). In the $CaMgSi_2O_6$-rich portion of the join, clinopyroxene forms elongated prismatic crystals up to 100 μm in length (Fig. 1c, d). In the $KAlSi_3O_8$-rich portion of the join, clinopyroxene forms both clusters of small crystals and relatively large anhedral crystals in the products of quenching (Fig. 1e). At the solidus, clinopyroxene forms acicular crystals (Fig. 1f). As a rule, garnet grains are equant (Fig. 1d). In the experiments produced in the diopside-rich portion of the join at temperatures 1,000–1,100°C, garnet form large (up to 100 μm in diameter) euhedral crystals and locally includes clinopyroxene. Sanidine forms large subhedral crystals (up to 100–300 μm) containing clinopyroxene inclusions (Fig. 1e). In the high-temperature experiments, sanidine crystals are surrounded by quench zones and contain "quench pockets", which are composed of acicular sanidine intermixed with residual glass (Fig. 1e). At lower temperatures, sanidine crystallizes as euhedral grains (Fig. 1f).

All experiments contain quenched aluminosilicate melt. In the experiments conducted at temperatures above 1,200°C at 6 GPa and above 1,000°C at 3.5 GPa, the quenched melt appears as relatively homogeneous bubble-free glasses resulting from rapid quenching (about 300–400°C/s). Locally, there are aggregates of acicular crystals, irregularly dispersed in the homogeneous glass (Fig. 1 c, d). Glass is extremely rare in the experiments near the inferred solidus. In most cases, the products of the melt quenching near the solidus are aggregates of acicular crystals.

Specific zoned distribution of phase assemblages is characteristic for the experiments containing Grt, Cpx, San, and quenched melt (experiments 1089, 1090, 1121; Table 1). For example, experiment 1090 shows three zones (from bottom to top of Fig. 2a): (1) the Cpx + Grt + glass zone, (2) the glassy zone, and (3) the Cpx + San + Q zone. The zone (1) is an aggregate of subhedral clinopyroxene grains intergrown with garnet (Fig. 2b). The Cpx + San + Q zone is composed of subhedral San and Cpx grains with "pockets" of quenching textures (Fig. 2c). Textures of both zones resemble a cumulate of crystals in the melt. This appearance would imply a

gravitational separation of phases during long-time runs (4–6 h): phases of higher density (Grt and Cpx) settle onto the capsule bottom, whereas lower-density sanidine tends to float up. Similar Cpx and Grt aggregation on the capsule bottom is observed in some San-free experiments, as well.

Partial replacement of large sanidine crystals with aggregates Cpx + quench is identified in the experiments 1046, 1086, 1087, and 1194 (Table 1; Figs. 1e and 2d). This texture would imply the schematic reaction San + melt → Cpx in progress. The formation of the texture is presumably related to kinetics of phase crystallization in the sanidine-rich portion of the join. Large euhedral sanidine crystals (up to 300 μm) in this portion of the join (Fig. 1e) may have been grown immediately after pressurization but in the course of heating (see the experimental procedure above); growing sanidine crystals captured separate diopside grains, as well. At the run conditions, crystalline sanidine appeared to be as the starting mineral. In the course of the experiment, sanidine was re-equilibrated by means of interaction with melt to form new clinopyroxene. Diopside shielded by sanidine does not display any reaction (Fig. 1e).

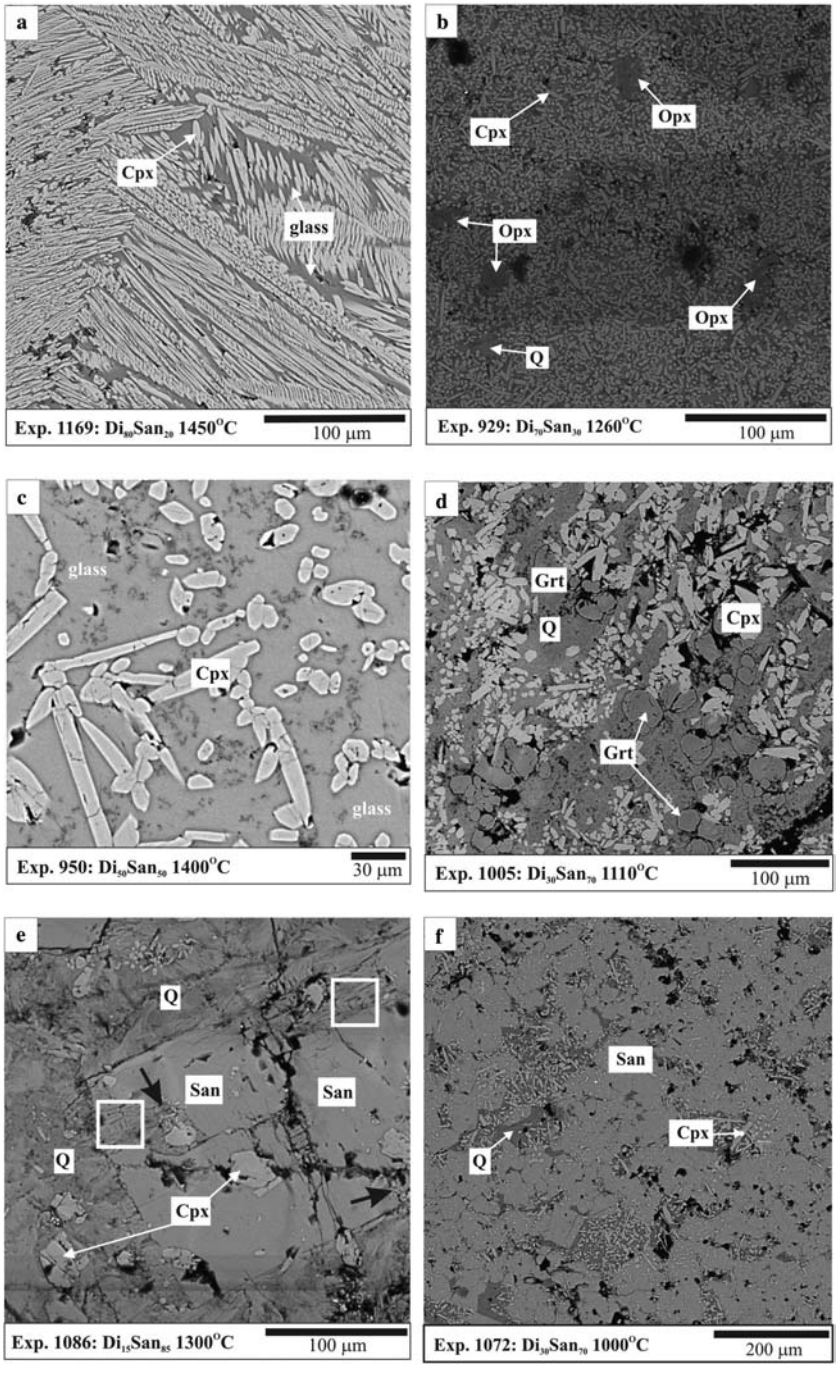


**Fig. 1** Textural phase relationships in the run samples synthesized in the join $CaMgSi_2O_6$–$KAlSi_3O_8$ at 6 and 3.5 GPa. **Plate a** Skeleton crystals of Cpx and $SiO_2$-rich glass. These textures create difficulties in identification of the liquidus in the $CaMgSi_2O_6$-rich portion of the join. **Plate b** Large euhedral Opx crystals and small Cpx crystals plunged into the quenching products (Q). **Plate c** Euhedral Cpx crystals in the aluminosilicate melt at the liquidus of the join. Darker areas in the glass are composed of acicular phases, the quenching products (Q). **Plate d** Crystals of Cpx and Grt in the matrix that is composed of quenched melt (Q). The quenched melt around some crystals is presented by homogeneous glass. **Plate e** Large San crystals and potassium-poor Cpx crystals shielded by the sanidine crystals. Quenching zones and "pockets" at the San crystals (indicated with *squares*) are composed of acicular aggregates of sanidine and residual glass. *Black arrows* mark the places, where sanidine crystals are partially replaced with the aggregates of K-bearing Cpx and quench. **Plate f** Euhedral sanidine and acicular clinopyroxene crystals at the solidus of the join $CaMgSi_2O_6$–$KAlSi_3O_8$ at 3.5 GPa. Sanidine grains contain numerous inclusions of clinopyroxene, giving an appearance of the eutectic-like texture; *gray* areas between sanidine crystal are quenching products (Q)

## Phase composition

The mean grossular content of *garnets* produced at 6 GPa varies from 20 to 35 mol% (Table 2). Garnets show either concentric (boundaries of zones are parallel to the crystal outlines) or spotty (Ca-rich zones form spots in the grains or are attached to the contacts with clinopyroxene) zoning. Grossular content in garnets from the experiment 1090 varies from 40 up to 55 mol% (Table 2). Centers of grains show lower $N_{Ca}$, while rims contacting to clinopyroxene are affected by a local increase of the grossular content (Fig. 1e). The zoning of garnets in this experiment (as well as in 1089), probably, resulted from re-equilibration of composition after settling of garnet on the capsule bottom during the run. No systematic variation of garnet composition with temperature is found, but garnets in experiments at the lowest temperatures (978 and 1037; Tables 1 and 2) are very Ca-rich ($N_{Ca} = 80$–$90$ mol%).

*Clinopyroxenes* synthesized at 6 GPa show the positive correlation of the K content with $Al^{M1}$–$Al^{IV}$ (Fig. 3a), which reflects the substitution $Mg^{M1} + Ca^{M2} \Leftrightarrow Al^{M1} + K^{M2}$ (e.g., Harlow 1997; Chudinovskikh et al. 2001; Safonov et al. 2002, 2003) and the presence of the KJd end-member in the clinopyroxenes. The K ⇔ Ca substitution into the M2 site of the clinopyroxene structure was also verified by the X-ray single-crystal refinements of two compositionally homogeneous crystal fragments from the experiments 1006 and 927, containing 0.60 and 0.81 wt% of $K_2O$, respectively. A notable excess of Al in the M1 site with respect to Ca-Ts and KJd (i.e., $Al^{M1}$–$Al^{IV}$–K) (Fig. 3a) is directly correlated as 2 : 1 with vacancies in the M2 site ($\square^{M2} = 1 - Ca - K - Mg^{M2}$) in most of clinopyroxenes (Fig. 3b). This correlation is evidence for the Ca-Esk end-member in KCpx. In the most cases, the $Al^{IV}$

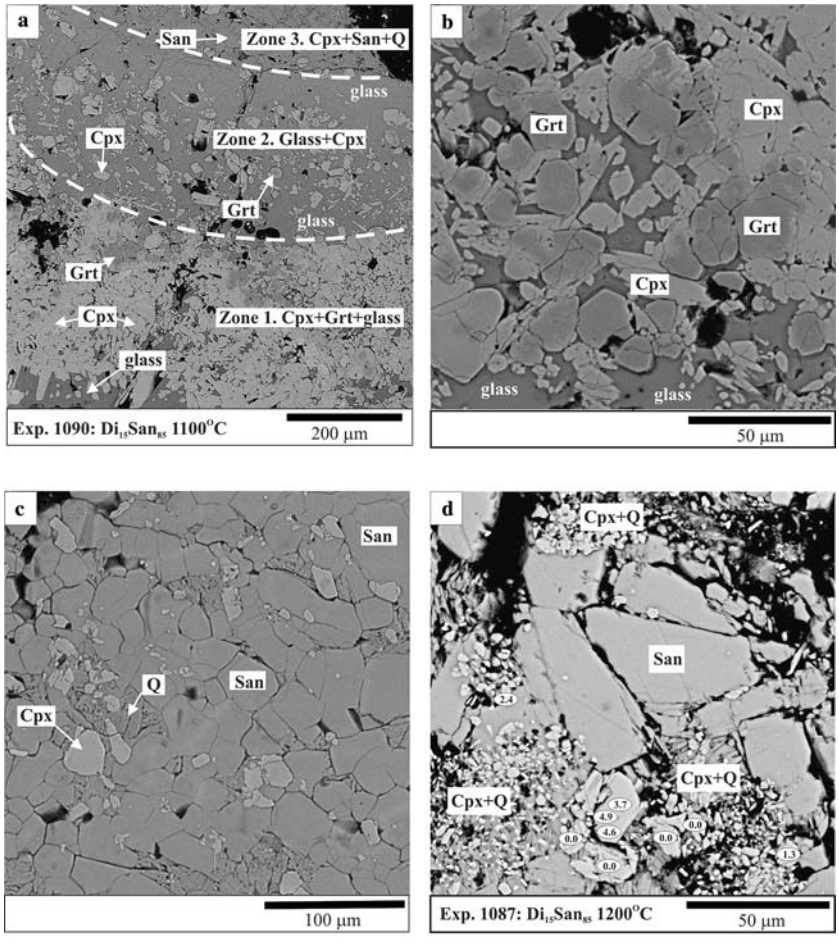


**Fig. 2** Specific textural features of the sanidine-bearing samples synthesized in the join $CaMgSi_2O_6$–$KAlSi_3O_8$ at 6 GPa. **Plate a** Zoned distribution of phase assemblages produced by separation of phases by gravity. Three zones are distinguished in the sample (from the bottom to the top): Zone 1—Cpx + Grt + glass; Zone 2—Cpx + glass (with rare Grt); and Zone 3—Cpx + San + quench. *Dashed lines* roughly mark boundaries between the zones. Relationships of phase in the first and the third zones are shown in plates 2b and 2c. These plates are outside of the plate 2a. **Plate b** Detailed view of the cumulate-like aggregates and intergrowths of Cpx and Grt with minor interstitial glass in the zone 1 in the Plate 2a. **Plate c** Detailed view of subhedral San and Cpx grains with "pockets" of quenching textures (Q) in the zone 3 in the Plate 2a; quenching textures are composed of acicular sanidine and residual glass. **Plate d** Replacement of San crystals with aggregates of Cpx + Q reflecting the assumed reaction San = KJd (in Cpx) + L in the $KAlSi_3O_8$-rich portion of the join. Numbers in the Cpx fields show the KJd content in this clinopyroxene (mol%)

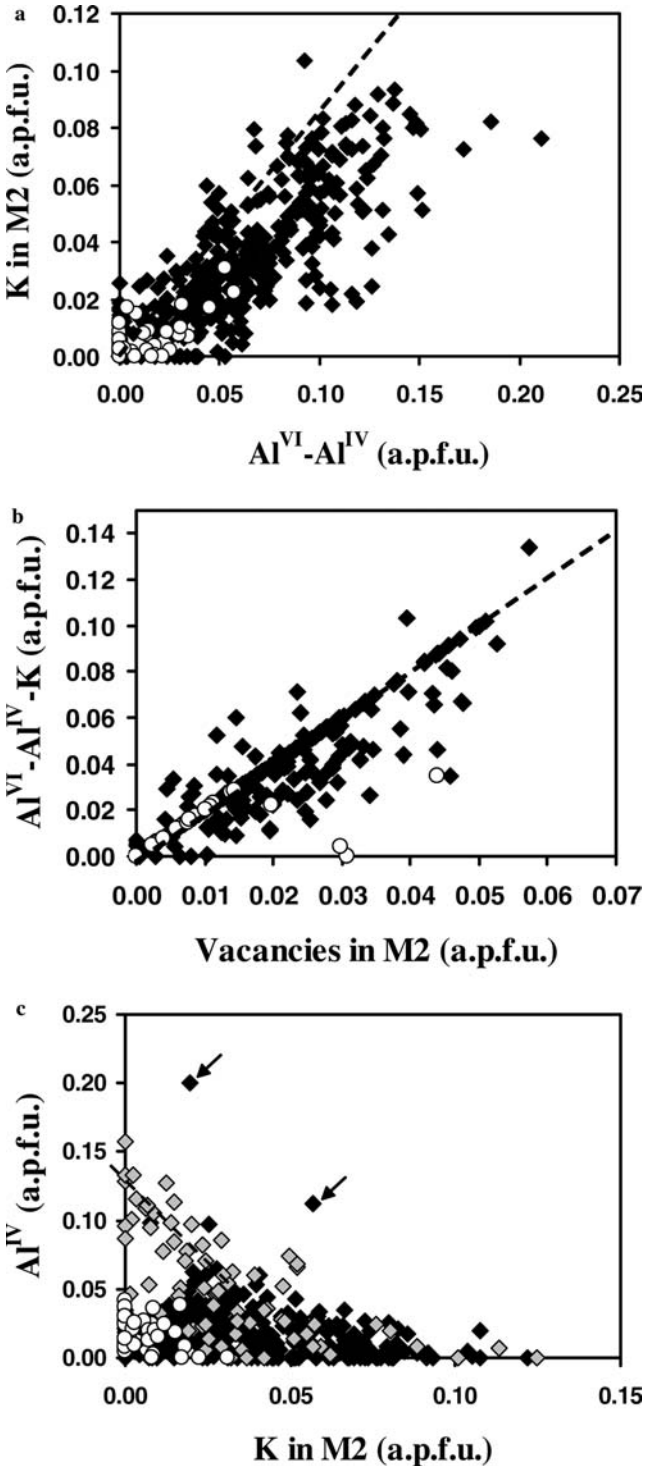


**Fig. 3** General compositional features of clinopyroxenes synthesized in the join $CaMgSi_2O_6$–$KAlSi_3O_8$ at 6 GPa (*black diamonds*) and 3.5 GPa (*white circles*). **a** Correlation of K in the M2 site with Al in the M1 site (excluding Al bound to the $CaAl_2SiO_6$ end-member). *Dashed line* shows a theoretical relation of these parameters corresponding to the two-site heterovalent isomorphism $Mg^{M1} + Ca^{M2} \Leftrightarrow Al^{M1} + K^{M2}$. **b** Correlation of vacancies in the M2 site with Al in the M1 site (excluding Al bound to the $CaAl_2SiO_6$ and $KAlSi_2O_6$ end-members). Dashed line shows a theoretical relation of these parameters corresponding to the two-site heterovalent isomorphism $Mg^{M1} + 0.5Ca^{M2} \Leftrightarrow Al^{M1} + 0.5\square^{M2}$. **c** Variation of $Al^{IV}$ and its negative correlation with K in the M2 site for clinopyroxenes enriched in Ca–Ts (*dashed line*). In this diagram, *black diamonds* show clinopyroxenes from the sanidine-free samples, while *gray diamonds* represent clinopyroxenes from the sanidine-bearing samples produced at 6 GPa. *Arrows* point to the clinopyroxenes included in garnets

content (i.e. Ca-Ts end-member) of clinopyroxenes does not exceed 0.05 a.p.f.u. (Table 2; Fig. 3c). The highest concentrations of $Al^{IV}$ up to 0.10–0.19 a.p.f.u. are characteristic for some cores of large Cpx crystals, Cpx inclusions in garnets, as well as Cpx intergrown with garnet in the sanidine-bearing experiments 1089, 1090, and 1121 (Table 2; Fig. 3c). For the Ca-Ts-rich clinopyroxenes, $Al^{IV}$ shows strong negative correlation with KJd (Fig. 3c). All clinopyroxenes contain Mg in the M2 site, i.e., CEn end-member (Table 2). Similar to the Ca-Ts end-member, highest CEn content is observed in cores of large clinopyroxene crystals and in clinopyroxenes included in garnets.

Thus, clinopyroxenes produced in the system $CaMgSi_2O_6$–$KAlSi_3O_8$ at 6 GPa are complex solid solutions of Di, KJd, Ca-Esk, CEn, and Ca-Ts. The KJd content of clinopyroxenes in the sanidine-free experiments produced at $N_{San}^{system} = 40$–70 mol% regularly increases upon decreasing temperature and reaches 10 mol% at ~1,000°C (Fig. 4). In contrast, the CEn content regularly decreases upon decreasing temperature. The Ca-Ts content tends to decrease slightly with decreasing temperature, whereas the Ca-Esk in clinopyroxenes is approximately constant at temperatures above 1,000°C.

The most interesting variations of composition are observed in Cpx in the sanidine-bearing experiments. The high temperature garnet-free experiment 1046 contains clinopyroxene with a mean KJd content about 5.7 mol% (Table 2), which is slightly higher than the KJd content in Cpx from the sanidine-free experiments at similar temperature (Fig. 4). In the experiments 1086, 1087, 1088, and 1194 (Table 1), large sanidine crystals include clinopyroxenes containing 0.0–0.4 wt% of $K_2O$, but no alumina to compensate potassium (Fig. 1e and Table 2). The irregular presence of uncompensated potassium in these clinopyroxene, probably, corresponds to K-fluorescence from sanidine and implies an absence of the KJd end-member. However, in addition to these clinopyroxenes (actually, diopside), experiments 1087 and 1194 (Table 1 and 2) contain relatively large clinopyroxene crystals enriched in KJd (4–8 mol%), Ca-Ts (2–7 mol%), and Ca-Esk (4–9 mol%). The detailed examination shows that KCpx grains are always coexist with the quenched melt, whereas diopside crystals are mostly associated with sanidine aggregates. Partially decomposed diopside grains are locally situated very close to subhedral KCpx grains, while aggregates of KCpx grains and quenched melt replace sanidine along grain boundaries (Fig. 2d). The zoned run samples 1121 and 1090 (Table 1) contain diopside as well, which is

surrounded by the sanidine aggregates (Fig. 2a, c). In addition to diopside, these samples contain Al-rich clinopyroxene in the Grt–Cpx cumulates and as separate crystals in glass (Fig. 1e). The Ca-Ts content varies within the range 4–7 mol%, but increases up to 15 mol% in contacts with garnet. The increase of the Ca-Ts content results in appreciable decrease of the KJd and Ca-Esk. Therefore, most of clinopyroxenes from the experiments 1090 and 1121 deviate from the general dependence of the KJd content on temperature (Fig. 4). Nevertheless, the concentration of the KJd component (about 5 mol%) in relatively low-Ca-Ts KCpx is in a good agreement with the general dependence in Fig. 4. Further reduction in temperature results in an increase of the KJd in clinopyroxene (e.g., experiments 1024 and 1136). The estimated KJd concentration in some clinopyroxenes from the experiments 1022 and 978 produced at temperatures 940 and 890°C (Table 1), respectively, reaches ~12 mol% (Table 2), which is consistent with the general dependence of the KJd content in KCpx on temperature, as well (Fig. 4). However, formulae of clinopyroxene from the experiment 1022 show a notable excess of Si over 2.0 a.p.f.u., probably, because of contamination with SWd. Therefore, its end-members cannot be estimated properly.

Thus, compositions of KCpx from the sanidine-bearing assemblages show a good correlation with temperature (Fig. 4). The deviations of the clinopyroxene compositions from this dependence can be explained by the significant textural inhomogeneity of the sanidine-bearing run samples.

Clinopyroxenes synthesized at 3.5 GPa show considerably lower KJd content (Table 2; Fig. 3a). Nevertheless, the potassium concentration in these clinopyroxenes increases with decreasing temperature as well. Just the run products 1072, obtained near the solidus (Table 1 and Fig. 1g), contain clinopyroxene with 0.6 wt% $K_2O$. However, we suggest that this apparent $K_2O$ concentration is mostly related to fluorescence from sanidine during microprobe analyses of these acicular crystals (Fig. 2). Clinopyroxenes produced at 3.5 GPa contain Ca-Esk, as well, but the concentration does not exceed 3 mol%.

*Orthopyroxene* from both the experiments 1159 and 929 contain up to 1.5 wt% of $Al_2O_3$ and CaO 1.2–2.5 wt% of CaO, suggesting low concentrations of Mg-Ts and Wol end-members (Table 2).

*Sanidine* composition in all experiments obeys the stoicheometry of $KAlSi_3O_8$. The total content of CaO and MgO content does not exceed 0.5 wt% (Table 2).

*Si-wadeite* in experiment 1022 (Tables 1 and 2) contains CaO, MgO, and $Al_2O_3$ with reduction in $K_2O$, which is interpreted as minute inclusions of clinopyroxene, garnet, and sanidine contaminants.

*Glasses* in all run products are characterized by relatively high $SiO_2$ (55–75 wt%), $Al_2O_3$ (11–19 wt%), and $K_2O$ (12–22 wt%) contents at CaO + MgO concentration less than 7 wt%. Composition of glasses produced at 6 GPa varies with temperature and bulk composition. For glasses synthesized in the diopside-rich portion of the join, the $SiO_2$ concentration is nearly constant, whereas it increases for glasses synthesized in the sanidine-rich portion. The join $K_2O$ slightly decreases with increasing temperature for all glasses. The $Al_2O_3$ content in glasses is approximately constant over the temperature range of experiments.

Using Raman spectroscopy, we verified the presence of water in glasses from experiments 950, 1011, and 1109 (Table 1). In addition to peaks in the low-frequency range corresponding to vibration of tetrahedral cations, spectra showed a wide band with a peak in the frequency range 3,500–3,550 $cm^{-1}$ attributed to stretching vibrations from molecular water (e.g., Holz

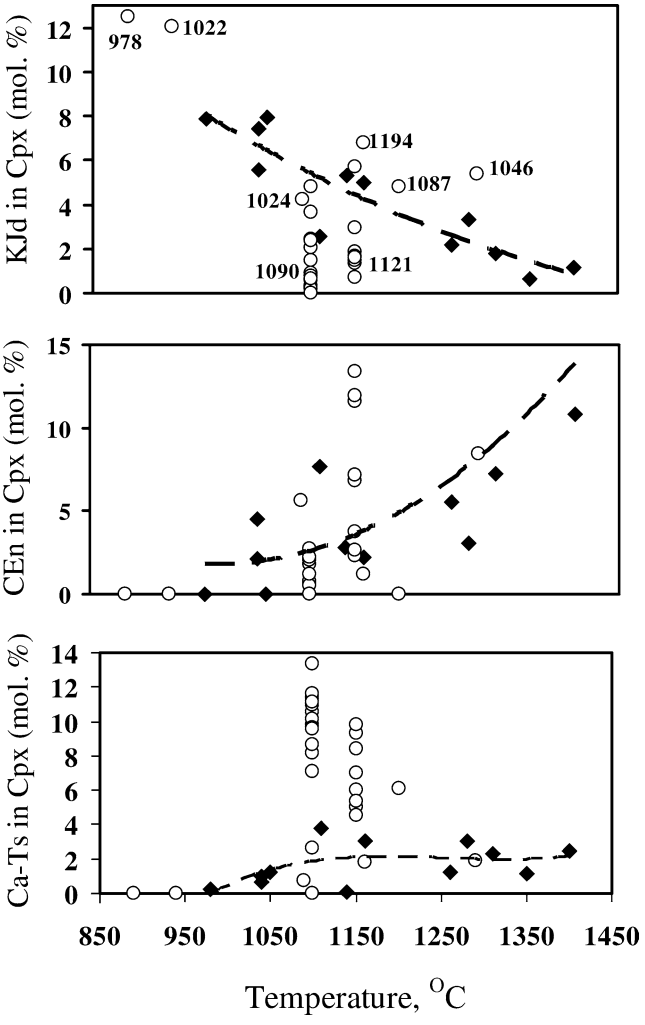


**Fig. 4** Temperature dependence of the mean KJd, CEn, and Ca-Ts contents for clinopyroxenes from sanidine-free samples (*black diamonds*) and sanidine-bearing samples (*white circles*) produced at 6 GPa. Labels indicate the sanidine-bearing run samples discussed in the text. For the experiments 1090 and 1121, all measured clinopyroxenes are plotted in order to demonstrate a variability of the clinopyroxene composition in these samples (see text). *Dashed lines* represent fits for clinopyroxene compositions from sanidine-free samples

et al. 1996). No bands of OH-groups, which would be expected at relatively high water content, were present in the spectra. Analyses of glasses usually show a total oxide concentration close to 100 wt% (Table 2), which implies low water concentration in these glasses, as well. Glass is very rare in the experiments produced at temperatures below 1,100°C, whereas products of the melt quenching are presented by aggregates of acicular crystals, probably, of mica-like phases. Analyses of these quenching aggregates show the total oxide concentration 95–97 wt% (Table 2). Their formation is related to local accumulation of water (since neither Cpx nor Grt and San contains water) in the residual melt. The presence of these quenching textures in the low-temperature experiments makes locating the solidus in T–X space difficult.

## *T–X* diagrams for the join $CaMgSi_2O_6$–$KAlSi_3O_8$ at 6 and 3.5 GPa

### Topology and T–X diagram for the join $CaMgSi_2O_6$–$KAlSi_3O_8$ at 6 GPa

The system Di–San at ambient pressure is a pseudobinary join within the system $CaMgSi_2O_6$–$KAlSi_2O_6$–$SiO_2$, characterized by crystallization of Lc at liquidus and peritectic reaction Lc + L = San (Schairer and Bowen 1938). At pressures above 2 GPa, sanidine melts congruently (e.g., Lindsley 1966) up to about 6.5 GPa. Sanidine is unstable at higher pressure with the formation of the assemblage SWd + Ky + Cos (Kinomura et al. 1975; Urakawa et al. 1994; Yagi et al. 1994; Akaogi et al. 2004). But diopside is stable and melts congruently up to pressure ~16 GPa (Gasparik 1996). Thus, our experiments (Table 1) were conducted within the stability fields of both the San and Di up to temperatures of their congruent melting.

Phase relations on the join $CaMgSi_2O_6$–$KAlSi_3O_8$ can be described in terms of the five-component system $K_2O$–CaO–MgO–$Al_2O_3$–$SiO_2$. As in our previous study (Safonov et al. 2003), we consider the four-component system $K_2O$–(Ca, MgO)–$Al_2O_3$–$SiO_2$ in order to simplify the topological analysis of the join. This simplification assumes that the Ca/Mg in garnets and clinopyroxenes is constant, while clinopyroxene is the only potassium-bearing solid solution. The true Ca/Mg is not constant in the crystallized phases (see below). However, this simplification allows derivation of a general topology of the join $CaMgSi_2O_6$–$KAlSi_3O_8$.

Phases at the solidus on the join Di-San at 6 GPa are $Cpx_{ss}$ (the Di–KJd–CEn–Ca–Esk–Ca–Ts solid solution), $Grt_{ss}$ (the Prp–Grs solid solution), and San. SWd was observed with $Cpx_{ss}$ + San in experiments at $N_{San}^{system}$ = 95 mol% (see experiment 1022 in Tables 1 and 2). $Opx_{ss}$ (the En–Mg–Ts–Wol solid solution) is identified in the $CaMgSi_2O_6$-rich portion of the system (Table 1), but its presence at the solidus is not confirmed. The $Cpx_{ss}$, $Grt_{ss}$, and SWd are products of reactions between starting Di and San:

$$1/3\,\mathrm{Di} + \mathrm{San} = 1/9\,\mathrm{Prp} + 2/3\,\mathrm{Ca} - \mathrm{Esk} + 1/9\,\mathrm{KJd} + 4/9\,\mathrm{SWd} \quad (4)$$

Compositions of Grt, KCpx, and SWd are located off the binary join Di–San, i.e., their compositions cannot be expressed as linear combination of the two end-member components (Di and San). This feature allows classification of the join as pseudobinary (Ehlers 1972; Maaløe 1985; Litvin 1991). The positions of Di, Grt, SWd, San compositions within the $K_2O$–(Ca,MgO)–$Al_2O_3$–$SiO_2$ tetrahedron are shown in Fig. 5a. These end-members define a smaller tetrahedron, one edge of which is the join Di–San. In addition, clinopyroxene is a complex solid solution of Di, KJd, Ca-Esk, CEn, and Ca-Ts, whose formation also results from reactions between the starting Di and San:

$$\mathrm{Di} + 3\,\mathrm{San} = \mathrm{KJd} + 2\,\mathrm{Ca} - \mathrm{Esk} + 1/2\,\mathrm{CEn} + \mathrm{SWd} \quad (5a)$$

$$\mathrm{Di} + 2\,\mathrm{San} = 1/3\,\mathrm{Ca} - \mathrm{Ts} + 4/3\,\mathrm{Ca} - \mathrm{Esk} + 1/2\,\mathrm{CEn} + \mathrm{SWd}. \quad (5b)$$

At relatively low temperatures, the CEn end-member exsolves from the $Cpx_{ss}$ to form a separate phase, i.e., the $Opx_{SS}$ (see experiments 929 and 1159 in Table 1 and Fig. 2a).

Reactions (4) and (5) contain SWd as a product phase. However, we surely identified SWd only at $N_{San}^{system}$ = 95 mol% (Table 1), but this phase was not observed in the dominant portion of the interpreted solidus. Si-wadeite could be unobserved because of its low content. However, since no traces of SWd were found during the special examination (repeated polishing and the BSE mapping), we assume that SWd is not stable in this portion of the join, because of its consummation to form additional KJd in the clinopyroxene solid solution:

$$1/3\,\mathrm{Prp} + 1/3\,\mathrm{Grs} + \mathrm{SWd} = 2/3\,\mathrm{KJd} + \mathrm{Di}\ (\text{for garnet} - \text{bearing assemblages}) \quad (6a)$$

$$\mathrm{Ca} - \mathrm{Ts} + 1/2\,\mathrm{CEn}\ (\text{or En}) + \mathrm{SWd} = \mathrm{Di} + 2\,\mathrm{KJd}\ (\text{for garnet} - \text{free assemblages}). \quad (6b)$$

In the San-rich portion of the join, the bulk composition is suitable for coexistence of SWd with KCpx and San.

Due to the formation of $Cpx_{SS}$ and $Opx_{SS}$, the large tetrahedron Di–Grt–SWd–San splits into pseudo-tetrahedra (Cpx + Opx)$_{SS}$, (Cpx + Opx)$_{SS}$–Grt, (Cpx + Opx)$_{SS}$–Grt–San, (Cpx + Opx)$_{SS}$–SWd, (Cpx + Opx)$_{SS}$–

Grt–SWd, and (Cpx + Opx)$_{SS}$–Grt–SWd–San (Fig. 5b), which correspond to subsolidus assemblages within the system Di–Grt–SWd–San. Similar to the join Di–Lc at 7 GPa (Safonov et al. 2003), owing to both the Cpx$_{ss}$ and the Opx$_{ss}$ formation, the beginning of a true join is slightly displaced inward of the (Cpx + Opx)$_{ss}$ tetrahedron. In addition, because of SWd formation, the end of the join is slightly shifted inward the large tetrahedron (Cpx + Opx)$_{ss}$–Grt–SWd–San, but is located very close to the San apex (the end of the join is further denoted as San*). Therefore, the Di–San serves as a fictive join. Displacement of the boundaries of the true join is another evidence of its pseudobinary character (Ehlers 1972; Maaløe 1985; Litvin 1991). Starting from some point inside the (Cpx + Opx)$_{ss}$ tetrahedron, the true Cpx$_{ss}$–San* join penetrates four tetrahedra (Fig. 5b): (Cpx + Opx)$_{ss}$, (Cpx + Opx)$_{ss}$–Grt, (Cpx + Opx)$_{ss}$–Grt–San, and (Cpx + Opx)$_{ss}$–Grt–SWd–San.

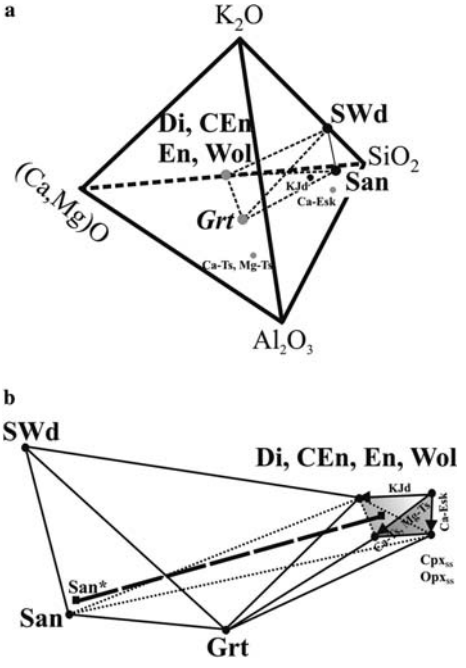


**Fig. 5** Topology of phase relations in the join $CaMgSi_2O_6$–$KAlSi_3O_8$ at 6 GPa (see explanation in the text). **a** Position of phases and end-members forming in the join $CaMgSi_2O_6$-$KAlSi_3O_8$ in the $K_2O$–(Ca, Mg)O–$Al_2O_3$–$SiO_2$ tetrahedron. *Solid lines* show visible tie-lines, while *dashed lines* indicate invisible tie-lines. *Black data points* are within the $K_2O$–$Al_2O_3$–$SiO_2$ plane. *Gray data points* are within the (Ca, Mg)O–$Al_2O_3$–$SiO_2$ plane. **b** Positions of the (Cpx + Opx)$_{SS}$–San* join (*thick dashed line*) with respect to phases and end-members in the system $CaMgSi_2O_6$–$KAlSi_3O_8$. *Gray tetrahedrons* denote the Cpx and Opx solid solutions: Di, CEn, KJd, Ca-Esk, Ca-Ts and En, Mg-Ts, Wol, respectively. *Arrows* are directed from Di (En) to other end-members of the Cpx$_{SS}$ and Opx$_{SS}$, whereas *black points* at the arrow ends schematically illustrate a maximal solubility of corresponding end-members in the Cpx$_{SS}$. *Black squares* schematically show a displacement of the beginning and the end of the true join (Cpx + Opx)$_{SS}$–San* inward both the (Cpx + Opx)$_{SS}$ and (Cpx + Opx)$_{SS}$–Grt–SWd–San tetrahedrons. *Solid lines* show visible tie-lines, while *dashed lines* indicate invisible (back-edge) tie-lines

The end of the join is located inside the (Cpx + Opx)$_{ss}$–Grt–SWd–San tetrahedron close to the San point. This position of the join Cpx$_{ss}$–San* corresponds to the following phase assemblages in the subsolidus: (Cpx + Opx)$_{ss}$, (Cpx + Opx)$_{ss}$–Grt, Cpx$_{SS}$–Grt–San, and Cpx$_{ss}$–Grt–SWd–San. Presence of Opx$_{ss}$ implies that the subsolidus region of at $N_{San}^{system} < 10$ mol% could split into free additional fields: Cpx$_{ss}$, Cpx$_{ss}$ + Opx$_{ss}$, and Cpx$_{ss}$ + Opx$_{ss}$ + Grt. In high-temperature experiments, either Cpx (in the diopside-rich portion of the join; Fig. 1c) or San (in sanidine-rich portion of the join) are found in glass. That implies that the join includes two liquidi only: Cpx$_{ss}$ and San. Opx$_{ss}$ was observed only at 1,200–1,260°C in the run products at $N_{San}^{system} <$ 30 mol% (runs 929 and 1159; Table 1), while it was not detected in the solidus at $N_{San}^{system} > 10$ mol%. This implies that Opx disappears at cooling, probably, via peritectic reaction to form the assemblage Cpx + Grt, so the Opx$_{ss}$ could be present in solidus only at $N_{San}^{system} < 10$ mol%. The assumed peritectic is very similar to that in the join Di–Prp at 3 GPa (O'Hara 1963), but occurs at lower temperature owing, probably, to the presence of the K–Si-rich melt. In the absence of Opx at higher temperature, the CEn end-member dissolves in Cpx$_{SS}$ (Fig. 4).

Thus, we established a possible sequence of phase fields in the subsolidus and implied liquidus relations in the join Cpx$_{ss}$–San* at 6 GPa. This allows construction of the *T*–*X* diagram using the data from Table 1 and the rules on construction of the diagrams for the pseudobinary systems (Rhines 1956). The pseudobinary join Cpx$_{ss}$–San*, which is a chemical analogue of the system $CaMgSi_2O_6$–$KAlSi_3O_8$, is characterized by the following features (Fig. 6).

1. Up to $N_{San}^{system} = 85$ mol%, Cpx$_{ss}$ is a liquidus phase. Only at the higher $N_{San}^{system}$ sanidine does become a liquidus phase.
2. The assemblage Opx$_{ss}$ + Cpx$_{ss}$ + L is stable in the $CaMgSi_2O_6$-rich portion of the join. Peritectic reaction Opx$_{ss}$ + Cpx$_{ss}$ + L = Cpx$_{ss}$ + Grt$_{ss}$ is proposed to explain the absence of Opx in the solidus at the $N_{San}^{system} > 10$ mol%.
3. The join Cpx$_{ss}$–San* is characterized by a wide field of the joint crystallization of Cpx and pyrope-grossular Grt, which corresponds to the Cpx$_{ss}$ + Grt$_{ss}$ + L cotectic.
4. Below the liquidus, sanidine is stable only at $N_{San}^{system} > 70$ mol%. The cotectic assemblages Cpx$_{ss}$ + San + L, Cpx$_{ss}$ + Grt$_{ss}$ + San + L, Cpx$_{ss}$ + San + SWd + L are stable in the sanidine-rich portion of the join.
5. The eutectic Cpx$_{ss}$ + Grt$_{ss}$ + San + SWd + L is situated very close to the San apex. The position of the entire solidus is unconstrained, because ambiguous interpretation of quenching textures related to the local accumulation of water in the low-temperature experiments. Position of the solidus line in Fig. 6 is conventional.

The phase diagram in Fig. 6 has to be considered as preliminary, because (1) the $CaMgSi_2O_6$-rich portion of the diagram is not well experimentally constrained and requires further experiments, especially for the Opx–Cpx–Grt relationships at the assumed peritectic and the solidus; (2) exact position of the solidus is not established. In addition, no variation of Ca-content of Grt and the CEn, Ca-Esk and Ca-Ts components in clinopyroxene are accounted for. These features cannot be clearly indicated on the 2D diagram for the multi-component system. Experimental data allow confirmation of the general topology of the join and specification of major phase fields, assumed from the topological analysis.

### Topology and the T–X diagram for the join $CaMgSi_2O_6$–$KAlSi_3O_8$ at 3.5 GPa

Grt and SWd are absent on the join Di–San at 3.5 GPa (Table 1). However, Cpx at this pressure also contains low concentrations of KJd, Ca-Esk, and CEn (Table 2; Fig. 3a, b). The introduction of these end-members in the $Cpx_{ss}$ results in the displacement of Cpx from diopside and, subsequently, from the Di–San tie-line. This feature corresponds to a slight deviation of the $Cpx_{ss}$–San join at 3.5 GPa from a truly binary join (Fig. 7). The topology of the join at 3.5 GPa is similar to the topology of the system Di–San–$H_2O$ at 1 GPa of water pressure characterized by the formation of the Di–Ca-Ts solid solution (Yoder and Upton 1971). Clinopyroxene is a liquidus phase at $N_{San}^{system} < 70$ mol%, whereas San crystallizes at liquidus at the higher $N_{San}^{system}$. Ternary eutectic Cpx + San + L occurs between 1,000 and 1,050°C.

## Discussion and application to the natural assemblages

Experiments at 6 and 3.5 GPa demonstrate that the K-rich melts in the system $CaMgSi_2O_6$–$KAlSi_3O_8$ could produce common mantle mineral assemblages, such as Cpx + Grt, Cpx + Opx, Cpx + San, or Cpx + Grt + San. At 6 GPa, the assemblage Grt + Cpx coexists with K–Al–Si-rich melt down to about of 1,000–1,100°C (Fig. 6). These temperatures are appreciably lower than temperatures of crystallization (at least above 1,300°C) for the assemblage Grt + Cpx from potassium-free melts, including Na and Fe-bearing systems (see Litvin 1991 and references therein for a review of the phase diagrams in model and natural eclogite systems). Even if we take into account the presence of the uncontrolled amount of water in the starting gels, the lowering of liquidi and solidi of sanidine-bearing system in comparison to the potassium-free systems is evident. Low solidus temperatures are caused probably by the high $SiO_2$ and $K_2O$ contents in the sanidine-bearing system and the polyphase composition of the subsolidus (increasing number of phases decreases the melting temperature for the eutectic). Relatively low temperature of the Cpx and Grt equilibria with the K–Al–Si-rich melts is in good agreement with mineral thermometry of deep-seated assemblages, which in the most cases indicate temperatures 1,250–1,300°C. Addition of Na, Fe, and other components would further lower temperatures for coexistence of Cpx, Grt, and Opx with K-rich melts at pressures of about 6 GPa.

Some natural eclogite assemblages bear evidence for equilibrium with potassium-rich aluminosilicate melts (Bulanova and Argunov 1985; Bulanova et al. 1988; Novgorodov et al. 1990), whose compositions were close to the melts that we have described in the system $CaMgSi_2O_6$–$KAlSi_3O_8$. One of the most important

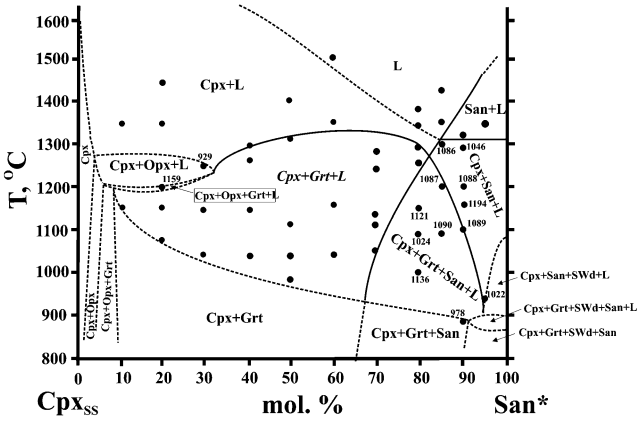


**Fig. 6** Preliminary phase *T–X* diagram for the system $CaMgSi_2O_6$–$KAlSi_3O_8$, i.e., join $Cpx_{SS}$–San* at 6 GPa. *Solid lines* denote experimentally established boundaries of phase fields; *dashed lines* indicate the assumed boundaries of phase fields; labeled data points relate to the specific experiments (Table 1) discussed in the text

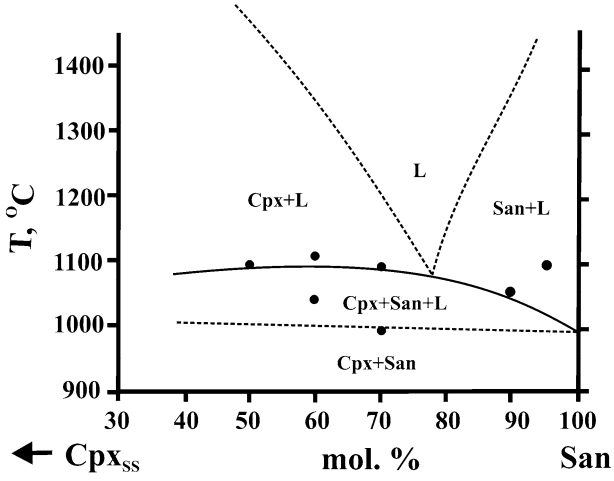


**Fig. 7** Preliminary *T–X* phase diagram for the system $CaMgSi_2O_6$–$KAlSi_3O_8$ (join $Cpx_{SS}$–San) at 3.5 GPa. *Solid lines* denote experimentally established boundaries of phase fields; *dashed lines* indicate the assumed boundaries of phase fields

features of the natural assemblages is the concentration of $K_2O$ in clinopyroxenes, which varies from 0.2 wt% in some eclogite xenoliths up to 1.4 wt% in clinopyroxene inclusions in diamonds (e.g. Stachel et al. 2000a). Using the negative effect of jadeite on the KJd solubility in the UHP Cpx, we demonstrated previously (Safonov et al. 2004) that the potassium-bearing omphacite inclusions in diamonds could crystallize from the potassium-rich melts at pressures below 6.5 GPa. Despite the presently low $K_2O$ content, many Cpx from eclogite xenoliths also show evidence for initially elevated potassium content, such as sanidine lamellae (Reid et al. 1976; Schulze and Helmsteadt 1988; Smith et al. 1991; Schmickler et al. 2004). Some melt inclusions in diamonds from kimberlites (Prinz et al. 1975; Bulanova and Argunov 1985; Bulanova et al. 1988; Novgorodov et al. 1990; Navon et al. 2003; Shiryaev et al. 2003) show high contents of $SiO_2$ (61–67 wt%), $Al_2O_3$ (7–21 wt%), and $K_2O$ + $Na_2O$ (6–18 wt%) at low concentration of CaO, MgO, FeO, and volatile components. These concentrations are also characteristics of the melts along the $CaMgSi_2O_6$–$KAlSi_3O_8$ join (Table 2). Inclusions of potassic aluminosilicate melts are commonly accompanied by Cpx, Grt, and San (Bulanova and Argunov 1985; Bulanova et al. 1988; Novgorodov et al. 1990), which are also major phases in the join $CaMgSi_2O_6$–$KAlSi_3O_8$ (Tables 1 and 2). These data allow application of our experimental results to reconstruction of the evolution of these natural assemblages.

Here we consider theoretically just two specific features of the evolution of potassic melts and their assemblages deduced from the present experimental results: (1) the relationships between KCpx and San and (2) the sequence of mineral crystallization from the K-rich melts. The detailed application of the experimental results for the K-rich aluminosilicate systems to natural assemblages will be discussed in subsequent publications.

## Relations between potassium-bearing clinopyroxene and sanidine

The phase diagram in Fig. 6 shows that only melts with $N_{San}^{system} > 70$ mol% are able to produce the assemblage Cpx + San at pressures close to the upper boundary of the sanidine stability. At the lower $N_{San}^{system}$, the Cpx + San assemblage is unstable because of the complex reactions (4)–(6), and Cpx is the only solid phase hosting potassium (Figs. 4 and 6).

In the San-bearing portion of the system, KCpx appears at ~1,300°C (experiment 1046; Fig. 6). The value $N_{KJd}^{Cpx} \sim 6$ mol% roughly agrees with $N_{KJd}^{Cpx}$ of San-free experiments at similar temperature (Fig. 4). The formation of almost pure Di associated with San in the experiment 1086 at similar temperature (Table 2) is, probably, related to shielding of diopside by large San crystals (Fig. 1e). This interpretation is readily supported by the presence of KCpx and diopside in this experiment, as well as in both the 1087 and 1194. KCpx forms separate crystals or clusters among the quench products. Thus, KCpx is in equilibrium with the melt. Similar texture, produced by separation of phases in the melt (see above), is characteristic also for the garnet-bearing experiments containing both KCpx and diopside (experiments 1089, 1090, 1121).

The experiments 1046, 1086, 1087, and 1194 display textures that are consistent with reaction relationships between Cpx, San, and melt (Figs. 1e and 2d). Figure 2d shows a partial replacement of San by the aggregate of KCpx ($N_{KJd}^{Cpx}$ up to 4.9 mol%) and quenched melt. Relics of semi-reacted diopside are locally preserved inside the KCpx + Q aggregates (Fig. 2d). The above texture corresponds to the following reaction:

$$\underset{\text{Di}}{(1-x)CaMgSi_2O_6} + \underset{\text{San}}{xKAlSi_3O_8} = \underset{\text{KCpx}}{(1-x)CaMgSi_2O_6 \cdot xKAlSi_2O_6} + \underset{\text{melt}}{xSiO_2} \quad (7)$$

However, no reaction is observed between shielded Di and San (Fig. 2c). This observation allows the conclusion that the formation of KCpx after San is not a solid-state reaction: it proceeds only in the presence of melt. Therefore, the reaction (7) can be rewritten with $CaMgSi_2O_6$ as a component of the coexisting melt. The large (up to 300 μm) San crystals and cumulates contain "pockets" of the quenched melt consisting of acicular sanidine and residual glass (Figs. 1f and 2c). The composition of this quench, however, is very different from the composition of the melt outside the cumulates (see Table 2 for analyses of glass and Q in the experiment 1090). The major difference is the higher $SiO_2$ content in the quenched melt from the "pockets" (70 vs. 56 wt%). Thus, at high $SiO_2$ content in the melt (high silica activity) at constant $P$ and $T$, the reaction (7) is strongly displaced to the left (see below).

Thus, our results are consistent with the suggestion that the formation of KCpx in the sanidine-bearing portion of the system $CaMgSi_2O_6$–$KAlSi_3O_8$ (Fig. 6) proceeded via the crystals-melt reaction (7). At x = 1 this reaction could be re-written as San = KJd + L, which has a form of a peritectic reaction. Although KCpx is formed as a result of the reaction (7), San does not totally react out. The Cpx composition is controlled by the solidus line in the $CaMgSi_2O_6$-rich portion of the system, which is roughly drawn in accordance with the general dependence of the Cpx composition on temperature (Fig. 4) and defines a maximal solubility of KJd in Cpx on isotherms at 6 GPa. Figure 6 indicates that in the sanidine-bearing portion of the join first KCpx appears via the reaction (7), if the sanidine liquidus crosses the isotherm about 1,300°C. The isotherm corresponds to ~5 mol% of KJd in Cpx. Therefore, this value is a minimal $N_{KJd}^{Cpx}$ in the equilibrium San + KCpx + L at 6 GPa. Below 1,300°C, KCpx is stable with San and melt, and $N_{KJd}^{Cpx}$ increases systematically with decreasing

temperature up to the maximal value of 12 mol% at T < 1,000°C (Fig. 4). Thus, reaction (7) proceeds to the right side with decreasing temperature. That also means that the equilibrium (2)

$$\mathrm{KJd\ (in\ KCpx)} + [\mathrm{SiO_2}]^{\mathrm{L/fl}} = \mathrm{San},$$

being a part of the reaction (7), displaces to the left side with decreasing temperature. The equilibrium (2) is an analogue of the equilibrium Jd + $SiO_2^L$ = Ab, which displaces to the left side with decreasing temperature because of the low entropy of jadeite with respect to Ab. By analogy, the KJd should also have low entropy relative to San (Vinograd et al. 2004). Lower KJd content of Cpx crystallized at 3.5 in comparison to Cpx produced at 6 GPa suggests displacement of reaction (2) to the left side with pressure.

In addition to $T$ and $P$, both the reactions (2) and (7) are functions of $a^L_{SiO_2}$, whose increase results in the decrease of $N^{Cpx}_{KJd}$ in presence of San (Fig. 8). The join Di–San in Fig. 8 divides the system (Ca + Mg)–(K + Al)–Si into two portions: the silica-poor Di–Ks–San and the silica-rich Di–San–Cos compositional fields. Taking to account the possible formation of the assemblage Ks + San instead of the $KAlSi_2O_6$ composition at 6 GPa and $T$ > 1,000°C (Liu 1987), we tentatively assume eutectic relations in the binary joins San–Ks and San–Cos, since (1) all the phases are stable, (2) melt congruently, and (3) do not form any solid solutions. In this case, the join Di–San is a thermal barrier. KCpx is stable only in the region Di–Ks–San, while K-poor Di is to be formed in the system Di–San–Cos. All melts within the region Di–Ks–San would follow the cotectic KCpx + San toward the eutectic KCpx + Ks + San + L. In contrast, all melts from the Di–San–Cos region would crystallize along the Di + San cotectic and ultimately solidify at the eutectic point Di + San + Cos + L. In order to demonstrate this rule, we plotted compositions of homogeneous glasses and silica-rich "quench pockets" from the sanidine-bearing experiments on Fig. 8. It demonstrates that the compositions of glasses in all San-bearing experiments correspond either to the Di–Ks–San region or very close to the Di–San tie-line. These melts are compatible with KCpx and would crystallize along the first path. The data point for "quench pockets" (the analyses from the run sample 1090; Table 2) is situated deep in the Di–San–Cos region. Thus, the melt from the "quench pockets" is compatible with K-poor diopside and would crystallize along the second path. The analyses show that the "quench pockets" situated inside big San crystals or cumulates (Figs. 1f and 2c) coexist with Di. High $a^L_{SiO_2}$ destabilizes KCpx in the assemblage with San.

Previously, we proposed that the equilibrium (2) shifting to the right with decompression and cooling explained the formation of San lamellae in Cpx from the Grt–Cpx rocks of the Kokchetav UHP Complex suggesting their magmatic origin (Perchuk and Yapaskurt 1998; Perchuk et al. 2002, 2003). Similar lamellae are common for Cpx from mantle xenoliths, as well (Reid et al. 1976; Smith et al. 1991; Schmickler et al. 2004). The present experiments provide an evidence for the "pseudo-peritectic" reaction at high pressures. According to these data, the formation of the San lamellae in Cpx could occur either with isobaric heating or with near isothermal decompression. For ascending mantle melts, the latter path is more plausible. Another mechanism of sanidine formation from KCpx is an increase of silica activity in the melt, which could occur because of a separation of the non-silicate constituents (carbonates, chlorides) from the initial complex magma, probably, by immiscibility (e.g., Perchuk et al. 2002).

## Sequence of mineral crystallization from potassic aluminosilicate melts

The experimental study of the join $CaMgSi_2O_6$–$KAlSi_3O_8$ shows different topologies at 6 and 3.5 GPa (Figs. 6 and 7). Therefore pressure defines a sequence of mineral crystallization from melts, whose composition is close to the join $CaMgSi_2O_6$–$KAlSi_3O_8$ during cooling and decompression. At $N^{system}_{San}$ < above 70 mol%, clinopyroxene is a liquidus mineral at 6 GPa (Fig. 6). $N^{Cpx}_{KJd}$ increases with cooling up to 10–12 mol% (Fig. 4). If cooling proceeds simultaneously with decompression, the $N^{Cpx}_{KJd}$ either could significantly drop (at rapid uplift), or be practically constant (at slow uplift). If cooling occurs at $P$ > 4 GPa, Grt joins KCpx subsequently (Fig. 6). Earlier KCpx crystals could be partially trapped by the growing garnet as inclusions. In the diopside-rich melts ($N^{system}_{San}$ < 40 mol%), garnet crystallizes at

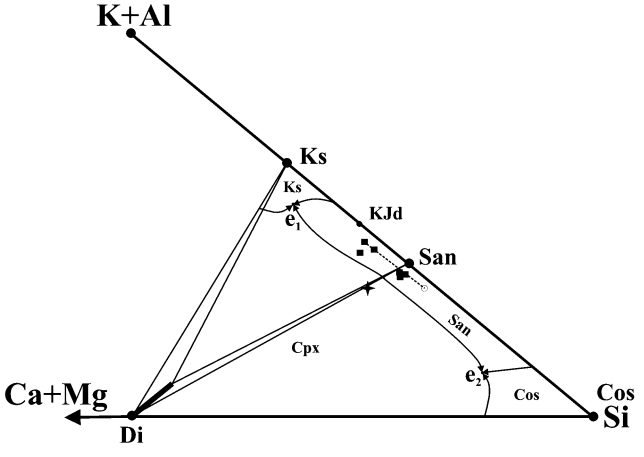


**Fig. 8** The portion of the triangle (Ca + Mg)–(K + Al)–Si showing mean compositions of homogeneous glasses (*black rectangles*) and "quench pockets" in the sanidine cumulates (*white circles*) from the sanidine-bearing samples with respect to the tie-line Di–San, Ks, and Cos. *Dashed line* connects compositions of glass and "quench pocket" from the sample 1090; *star* indicates composition of the melt over liquidus at 80 mol% of $KAlSi_3O_8$ in the system (run sample 1109; Tables 1 and 2); *thick line* shows the KCpx solid solution. Cotectic lines and eutectic points are arbitrary

relatively low temperatures (Fig. 6), and its amount in a rock would be significantly subordinate to Cpx. No San appears at HP in the melts at $N_{San}^{system} < 70$ mol% (Fig. 6). However, at $P < 4$ GPa, garnet does not crystallize, whereas San forms from the $CaMgSi_2O_6$-rich melts. The residual melt would crystallize to the eutectic assemblage of K-poor Cpx and San (Fig. 7, Perchuk and Yapaskurt 1998).

This scheme of crystallization was proposed by Perchuk et al. (2002, 2003) and Bindi et al. (2003) for the Ca–Fe rock varieties of Grt-Cpx rocks of the Kokchetav Complex, N. Kazakhstan, where Mg-number of clinopyroxene is below 55 mol%. However, in order to closely apply the results of the experiments in the Di–San join, we have to consider another rock variety, i.e. Mg-rich Grt–Cpx rocks of the same complex, where Mg-number of Cpx reaches 90 mol% (e.g. Sobolev and Shatsky 1990). Grt is quantitatively and texturally subordinate to Cpx, forming small rounded grains at the boundaries and inclusions in the peripheral zones of large Cpx crystals. In turn, Cpx inclusions in Grt are very rare. These inclusions contain variable concentration of $K_2O$ (0.4–0.7 wt%). The $K_2O$ content in the KCpx decreases from cores to rims of inclusions. Rare separate inclusions as well as cores of large Cpx crystals in matrix are crowded with K-feldspar lamellae. Later K- and lamellae-free Cpx form rims around the matrix Cpx. In addition to lamellae in Cpx, K-feldspar forms separate intergranular clusters between clinopyroxene and garnet grains.

Thus, the textural and compositional characteristics of the Mg-rich garnet–clinopyroxene rocks are very similar to the crystallization sequence for the melts in the diopside-rich portion of the join $CaMgSi_2O_6$–$KAlSi_3O_8$. Since primary San is absent in these rocks, we assume that crystallization of the rocks began at $P > 4$ GPa. KCpx with variable $K_2O$ contents crystallized during cooling and decompression. Grt joined Cpx subsequently. Because Grt was crystallized at a relatively later stage among larger clinopyroxene grains, the possibility of Cpx entrapment by Grt is very low. The wide variations of $K_2O$ content in KCpx inclusions, probably, points to their entrapment at very rapid cooling (resulting in increase of the potassium content) and decompression (resulting in decrease of the potassium content). Coexistence of potassium feldspar with K-poor Cpx corresponds to a final stage of magmatic evolution at $P < 4$ GPa.

The Cpx contents in both the Cpx–Grt–San and Cpx–Opx–Grt–San xenoliths from kimberlites are also above 40 vol% (Reid et al. 1976; Schmickler et al. 2004). Small grains of Grt, Opx, and San occur at the boundaries of large clinopyroxene crystals, and lamellae in Cpx crystals (e.g. Schmickler et al. 2004). All these textural features correspond to crystallization of Grt, Opx, and San later than Cpx and agree with the above scheme of crystallization from aluminosilicate melts of the diopside-rich portion of the join $CaMgSi_2O_6$–$KAlSi_3O_8$.

The characteristic feature of the above rocks is cumulate-like texture, which implies a fractionation of minerals during the crystallization process. Cumulates are composed of clinopyroxene and garnet, whereas sanidine and other K–Si-rich minerals occupy intergranular aggregates. Textures in some experiments of the join $CaMgSi_2O_6$–$KAlSi_3O_8$ (Fig. 2a–c) suggests a possibility of gravitational phase separation in the K-rich aluminosilicate melts, which produces Cpx + Grt cumulates cemented with the quenching products of the melt. We previously noted similar Cpx + Grt accumulation in the experiments for the join $CaMgSi_2O_6$–$KAlSi_2O_6$ at 7 GPa (Safonov et al. 2002, 2003). The major characteristics of melts both in the present join and in the join $CaMgSi_2O_6$–$KAlSi_2O_6$ are high concentration of $SiO_2$, $Al_2O_3$ and $K_2O$. It is well known that the viscosity of highly polymerized at ambient pressure melts rapidly *decreases* by orders of magnitude with pressure (e.g., Kushiro 1981; Persikov 1991). Therefore, the gravitational mechanism of Cpx, Grt, and San separation is physically substantiated for the UHP conditions. Our experimental results visualize this mechanism.

According to our results (Figs. 6 and 7), early (liquidus) crystallization of San at 6 GPa is possible only from very K–Al–Si rich melts. The rare findings of primary inclusions of San or its intergrowths with Cpx or Grt in diamonds (Prinz et al. 1975; Meyer and McCallum 1986; Bulanova and Argunov 1985; Novgorodov et al. 1990; Sobolev et al. 1998) correlates with scarcity of the K-rich aluminosilicate melt inclusions in diamonds (Prinz et al. 1975; Bulanova and Argunov 1985; Bulanova et al. 1988; Novgorodov et al. 1990; Shiryaev et al. 2003; Navon et al. 2003). Probably, the formation of San-producing melts at HP conditions is related to the late-stage evolution of more abundant mantle potassium-rich liquids of the carbonate–aluminosilicate–brine system (e.g., Navon et al. 2003 and references therein).

## Conclusions

This experimental study of the join $CaMgSi_2O_6$–$KAlSi_3O_8$ at 6 and 3.5 GPa allows the following major conclusions.

1. Melts with compositions close to the system $CaMgSi_2O_6$–$KAlSi_3O_8$, can produce a wide spectrum of eclogite-like assemblages involving Cpx, Grt, Opx, and San. Because of high $K_2O$ and $SiO_2$ contents, these melts coexist with Grt, potassium-bearing Cpx, and San down to ~1,100°C. This conclusion allows substantiation of a magmatic origin for mantle parageneses containing potassium-bearing Cpx or Cpx + San at $T < 1{,}200$°C.
2. Potassium-bearing Cpx or San are two major competing K-bearing phases within the "dry" UHP assemblages. San is unstable in the eclogitic (diopside-rich) melts at $P \sim 6$ GPa, being replaced by the assemblage of potassium-bearing Cpx (±Opx) and

Grt. In addition to the San instability in the peridotite systems (e.g., Wendlandt and Eggler 1980), this could be a major reason for extreme scarcity of San in the mantle assemblages. In contrast, Cpx becomes a major host of $K_2O$ at *P* down to about 4 GPa.

3. Liquidus crystallization of San and its assemblage with the KCpx and Grt at the UHP environments corresponds to the evolution of the extremely potassic and silica-rich aluminosilicate melts. These conclusions characterize the ultrapotassic melts as active participants of magmatic processes in the mantle, which dramatically change thermodynamic conditions of the formation of the "ordinary" deep-seated assemblages.

**Acknowledgements** Comments by George Harlow, Robert Luth, and Roland Stalder improved the text of the paper. The authors are very grateful to Ludmila P. Red'kina for preparation of starting materials and mixtures. We thank Alexei N. Nekrasov and Konstantin V. Van for providing facilities for electron microprobe analyses and Galina V. Bondarenko for Raman analyses of glasses. The study is supported by the Russian Foundation for Basic Research (projects 04-05-64896 to OGS, 02-05-64684 to YAL, and 02-05-64025 to LLP), the Program for young scientists of the Russian Academy of Science (project no. 323 to OGS), the RF President's Leading Scientific Schools Program (project no. 1645.2003.5 to LLP), the RAS Project no. 7 for High-Pressure Research (to YAL), and the Europea Academia (to OGS).

## References


Akaogi M, Kamii N, Kishi A, Kojitani H (2004) Calorimetric study on high-pressure transition in $KAlSi_3O_8$. Phys Chem Miner 31:85–91

Bindi L, Safonov OG, Litvin YA, Perchuk LL, Menchetti S (2002) Ultrahigh potassium content in the clinopyroxene structure: an X-ray single-crystal study. Eur J Miner 14:929–934

Bindi L., Safonov OG, Yapaskurt VO, Perchuk LL, Menchetti S (2003) Ultrapotassic clinopyroxene from the Kumdy-Kol microdiamond mine, Kokchetav Complex, Kazakhstan: occurrence, composition and crystal–chemical characterization. Am Mineral 88:464–468

Bradley CC (1969) High-pressure methods in solid state research. Butterworths, London

Bulanova GP, Argunov KP (1985) Inclusions of K-feldspar in diamond crystal from the "Mir" pipe. Dokl Akad Nauk SSSR Earth Sci 284:953–956

Bulanova GP, Novgorodov PG, Pavlova LA (1988) First finding of melt inclusion in diamond of the "Mir" pipe. Geochem Int 756–765

Chudinovskikh LT, Zharikov VA, Ishbulatov RA, Matveev YA (2001) On the mechanism of incorporation of ultra-high amounts of potassium into clinopyroxene at high pressure. Dokl Akad Nauk SSSR Earth Sci 380:1–4

Davies R, Harlow GE (2002) The high-pressure stability of K-cymrite and phases in the system Or-$H_2O$. EOS Trans AGU 83:F1455

Ehlers E.G. (1972) The interpretation of geological phase diagrams. WH Freeman and Company, San Francisco

Gasparik T (1996) Melting experiments on the enstatite–diopside join at 70–224 kbar, including the melting of diopside. Contrib Mineral Petrol 124:139–153

Hamilton DL, Henderson CMB (1968) The preparation of silicate compositions by a gelling method. Mineral Mag 36:832–838

Harlow GE (1997) K in clinopyroxene at high pressure and temperature: an experimental study. Am Mineral 82:259–269

Harlow GE (1999) Interpretation of KCpx and CaEs in clinopyroxene from diamond inclusions and mantle samples. Proceedings of the seventh international kimberlite conference, Vol 1. Cape Town, South Africa

Holz F, Bény J-M, Mysen BO, Pichavant M (1996) High-temperature Raman spectroscopy of silicate and aluminosilicate hydrous glasses: implication for water speciation. Chem Geol 128:25–39

Homan CG (1975) Phase diagram of Bi up to 140 kbars. J Phys Chem Solids 36:1249–1254

Kennedy CS, Kennedy GC (1976) The equilibrium boundary between graphite and diamond. J Geophys Res 81:2467–2470

Kinomura N, Kume S, Koizumi M (1975) Synthesis of $K_2SiSi_3O_9$ with silicon in 4- and 6-coordination. Mineral Mag 40:401–404

Kushiro I (1981) Change in viscosity with pressure of melt in the system $CaO–Al_2O_3–SiO_2$. Carnegie Institute Washington Year Book, pp 339–341

Lindsley DH (1966) Melting relations of $KAlSi_3O_8$: effect of pressures up to 40 kilobars. Am Mineral 51:1793–1799

Litvin YA (1991) Physical and chemical studies of melting of materials from the Deep Earth (in Russian). Nauka Press, Moscow

Liu L (1987) High-pressure transition of potassium aluminosilicates with an emphasis on leucite. Contrib Mineral Petrol 95: 1–3

Luth RW (1997) Experimental study of the system phlogopite–diopside from 3.5 to 17 GPa. Am Mineral 82:1198–1209

Maaløe S (1985) Principles of igneous petrology. Springer, Berlin Heidelberg New York Tokyo

Massone H-J, Dobrozhinetskaya L, Green HW II (2000) Quartz-K-feldspar intergrowths enclosed in eclogitic garnet and omphacite. Are they pseudomorphs after coesite? Ext. Abstract, The 31st Geological Congress, Rio de Janeiro, Brazil, p 4

Mathias M, Siebert JC, Rickwood PC (1970) Some aspects of the mineralogy and petrology of ultramafic xenoliths in kimberlite. Contrib Mineral Petrol 26:75–123

Meyer HOA, McCallum ME (1986) Mineral inclusions in diamonds from the Sloan kimberlites, Colorado. J Geol 94: 600–612

Navon O, Izraeli ES, Klein-BenDavid O (2003) Fluid inclusions in diamonds—the carbonatitic connection. The 8th international kimberlite conference, long abstract:FLA_0107

Novgorodov PG, Bulanova GP, Pavlova LA, Mikhailov VN, Ugarov VV, Shebanin AP, Argunov KP (1990) Inclusions of potassic phases, coesite and omphacite in the coated diamond crystal from the "Mir" pipe. Dokl Akad Nauk SSSR Earth Sci 310:439–443

O'Hara MJ (1963) The join diopside–pyrope at 30 kilobars. Carnegie Institute Washington Year Book, pp 116–118

Perchuk LL, Yapaskurt VO (1998) Mantle-derived ultrapotassic liquids. Russ Geol Geophys 39:1746–1755

Perchuk LL, Sobolev NV, Yapaskurt VO, Shatsky VS (1996) Relics of potassium-bearing pyroxenes from diamond-free pyroxene-garnet rocks of the Kokchetav massif, northern Kazakhstan. Dokl Akad Nauk SSSR Earth Sci 348:790–795

Perchuk LL, Safonov OG, Yapaskurt VO, Barton JM Jr (2002) Crystal-melt equilibria involving potassium-bearing clinopyroxene as indicators of mantle-derived ultrahigh-potassic liquids: an analytical review. Lithos 60(3–4):89–111

Perchuk LL, Safonov OG, Yapaskurt VO, Barton JM (2003) Reply to comments by Y. Zhu: K-feldspar in clinopyroxene from Grt–Cpx silicate rocks of the Kokchetav Massif. Lithos 68:121–130

Persikov ES (1991) The viscosity of magmatic liquids: experiment, generalized patterns. A model for calculation and prediction. Applications. In: Perchuk LL, Kushiro I (eds) Physical chemistry of magmas, advances in physical geochemistry, Vol 9. Springer, Berlin Heidelberg New York, pp 1–40

Prinz M, Manson DV, Hlava PF, Keil K (1975) Inclusions in diamonds: garnet lherzolite and eclogite assemblages. Phys Chem Earth 9:797–815

Reid AM, Brown RW, Dawson JB, Whitfield GG, Siebert JC (1976) Garnet and pyroxene compositions in some diamondiferous eclogites. Contrib Mineral Petrol 58:203–220

Rhines FN (1956) Phase diagrams in metallurgy. McGraw-Hill, New York

Ringwood AE, Reid AF, Wadsley AD (1967) High-pressure $KAlSi_3O_8$, an aluminosilicate with sixfold coordination. Acta Crystallogr 23:1093–1095

Safonov OG, Matveev YA, Litvin YA, Perchuk LL (2002) Experimental study of some joins of the system $CaMgSi_2O_6$–$(Ca,Mg)_3Al_2Si_3O_{12}$– $KAlSi_2O_6$–$K_2(Ca,Mg)(CO_3)_2$ at 5–7 GPa in relation to the genesis of garnet–clinopyroxene–carbonate rocks of the Kokchetav Complex (Northern Kazakhstan). Petrology 10:519–539

Safonov OG, Litvin YA, Perchuk LL, Bindi L, Menchetti L (2003) Phase relations of potassium-bearing clinopyroxene in the system $CaMgSi_2O_6$–$KAlSi_2O_6$ at 7 GPa. Contrib Mineral Petrol 146:120–133

Safonov OG, Litvin YA, Perchuk LL (2004) Synthesis of omphacites and isomorphic features of clinopyroxenes in the system $CaMgSi_2O_6$–$NaAlSi_2O_6$–$KAlSi_2O_6$. Petrology 12:84–97

Schairer JF, Bowen NL (1938) The system leucite–diopside–silica. Am J Sci 35:8

Schmickler B, Jacob DE, Foley SF (2004) Eclogite xenoliths from the Kuruman kimberlites, South Africa: geochemical fingerprinting of deep subduction and cumulate processes. Lithos 75:173–207

Schulze DJ, Helmstaedt H (1988) Coesite–sanidine eclogite from kimberlite: products of mantle fractionation or subduction?. J Geol 96:435–443

Schulze DJ, Valley JV, Spicuzza MJ (2000) Coesite eclogites from the Roberts Victor kimberlite, South Africa. Lithos 54:23–32

Shatsky VS, Sobolev NV (2003) The Kokchetav massif of Kazakhstan. In: Carswell DA, Compagnoni R (eds) Ultrahigh pressure metamorphism, EMU notes in mineralogy, Vol 5, pp 23–52

Shiryaev A, Izraeli ES, Hauri EH, Galimov EM, Navon O (2003) Fluid inclusions in Brazilian coated diamonds. The 8th international Kimberlite conference, long abstract: FLA_0115

Smith CB, Ramos ZN, Hatton CJ, Horsch H, Damarupurshad A (1991) Eclogite xenolith with exsolved sanidine from the Proterozoic Kuruman Kimberlite Province, Northern Cape, RSA. The 5th Kimberlite Conference, Ext Abstr pp 383–384

Smyth JR, Hatton CJ (1977) A coesite–sanidine grospydite from the Roberts Victor kimberlite. Earth Planet Sci Lett 34:284–290

Sobolev NV, Shatsky VS (1990) Diamond inclusions in garnets from metamorphic rocks: a new environment for diamond formation. Nature 343:742–746

Sobolev NV, Yefimova ES, Channer DM De R et al (1998) Unusual upper mantle beneath Guaniamo, Guyana Shield, Venezuela: evidence from diamond inclusions. Geology 26: 971–974

Spetsius ZV, Nikishov KN, Makhotko VF (1984) Kyanite eclogite with sanidine from the ''Udachnaya'' kimberlite pipe. Dokl Akad Nauk SSSR Earth Sci 279:117–180

Spivak AV, Litvin YA (2004) Diamond synthesis in multicomponent carbonate–carbon melts of natural chemistry: elementary process and properties. Diamond Relat Mater 13:482–487

Stachel T, Brey GP, Harris JW (2000a) Kankan diamonds (Guinea) I: from the lithosphere down to the transition zone. Contrib Mineral Petrol 140:1–15

Stachel T, Harris JW, Brey GP, Joswig W (2000b) Kankan diamonds (Guinea) II: lower mantle inclusion parageneses. Contrib Mineral Petrol 140:16–27

Thompson P, Parsons I, Graham CM, Jackson B (1998) The breakdown of potassium feldspar at high water pressures. Contrib Mineral Petrol 130:176–186

Urakawa S, Kondo T, Igawa N et al (1994) Synchrotron radiation study on the high-pressure and high-temperature phase relations of $KAlSi_3O_8$. Phys Chem Miner 21:387–391

Vinograd VL, Safonov OG, Winkler B (2004) Mixing properties of $CaMgSi_2O_6$–$KAlSi_2O_6$–$NaAlSi_2O_6$ clinopyroxenes determined from static lattice energy minimization calculations. EOS Trans AGU 85(17), Jt Assem Suppl, Abstracts, V54A-06

Wang W (1998) Formation of diamond with mineral inclusions of ''mixed'' eclogite and peridotite paragenesis. Earth Planet Sci Lett 160:831–843

Wang W, Takahashi E (1999) Subsolidus and melting experiments of a K-rich basaltic composition to 27 GPa: implication for behavior of potassium in the mantle. Am Mineral 84:357–361

Wendlandt RF, Eggler DH (1980) Stability of sanidine + forsterite and its bearing on the genesis of potassium magmas and the distribution of potassium in the upper mantle. Earth Planet Sci Lett 51:215–220

Wohletz KH, Smyth JR (1984) Origin of a Roberts Victor sanidine–coesite grospydite: thermodynamic considerations. In: Kornprobst J (ed) Kimberlites II: the mantle and crust–mantle relationships. Elsevier, Amsterdam, pp 33–42

Yagi A, Suzuki T, Akaogi M (1994) High-pressure transition in the system $KAlSi_3O_8$–$NaAlSi_3O_8$. Phys Chem Minerals 21:12–17

Yoder HS, Upton BGJ (1971) Diopside–sanidine–$H_2O$ at 5 and 10 kb. Carnegie Ins Wash Year Book 70:108–112

Zhang RY, Liou JG, Ernst WG, Coleman et al (1997) Metamorphic evolution of diamond-bearing and associated rocks from the Kokchetav Massif, northern Kazakhstan. J Metamorph Geol 15: 479–496